Supplemental Information

Supplemental Experimental Methods

Reagents and antibodies

LA1 was purchased from Chembridge Corp (Cat. No. 5679982, San Diego, CA). The anti-CD11b monoclonal antibody (mAb) 44a (IgG2a) (1) and the heterodimer-specific anti-CD18 mAb IB4 (IgG2a) (2) were from ATCC. The isotype control antibodies clone X40 (IgG1) and clone X39 (IgG2a), FITC-conjugated mAbs A85-1 (rat anti-mouse IgG1), R19-15 (rat anti-mouse IgG2a) were from BD Pharmingen (San Diego, CA), and the FITC-conjugated goat anti-mouse immunoglobulin (cat# A11029) was from Invitrogen (Carlsbad, CA). The rat anti-mouse anti-CD11b mAb M1/70 (IgG2b) (3) was purchased from the monoclonal antibody core at University of California, San Francisco (UCSF). Primary antibodies used in western blot were as follows: anti-phospho IKK-α/β (cat# 2078), anti-IKK-β (cat# 8943), anti-phospho p65/NF-kB (cat# 3036), anti-MyD88 (cat# 4283), anti-GAPDH (cat# 2118), anti-phospho AKT (cat# 4060), anti-AKT (cat# 4691), anti-phospho Fox01/03a (cat# 9464), anti-FOXO3a (cat# 2497), anti-phospho IRF3 (cat# 4947), anti-IRF3 (cat# 4302), anti-phospho IRF7 (cat# 14767), anti-phospho c-Cbl (cat# 8869), c-Cbl (cat# 8447), anti-phospho Src (cat# 6943), and anti-Src (cat# 2108) and were purchased from Cell Signaling Technologies, Danvers, MA. Other antibodies used were anti-rabbit IgG-HRP conjugate (cat# W4011, Promega, Madison, WI), anti-mouse IgG-HRP conjugate (cat# W4021, Promega, Madison, WI), anti-NF-kB (cat# 16502, Abcam, Cambridge, MA), and anti-IRF7 (cat# PA5-20280, Thermo Scientific, Waltham, MA). Human Fibrinogen (Plasminogen, von Willebrand Factor and Fibronectin depleted) was from Enzyme Research Laboratories (South Bend, IN), bovine serum albumin (BSA)

was from Sigma (St. Louis, MI) and the recombinant human ICAM1-Fc was from R&D Systems (Minneapolis, MN). The Highbind 384-well plates were obtained from Corning (Corning, NY). Non-fat milk was obtained from BioRad (Hercules, CA). PCR reagents, and restriction and modification enzymes were obtained from New England Biolabs Inc. (Beverly, MA). Glutathione-beads were purchased from Sigma (St. Louis, MI). All cell culture reagents were from Invitrogen Corp. (San Diego, CA). LPS (cat# tlrl-eklps), R848 (cat# tlrl-r848), polyI:C (pI:C, cat# tlrl-plc) and CpG (cat# tlrl-2216) were purchased from Invivogen (San Diego, CA). Human and mouse recombinant cytokines and ELISA kits were purchased from R&D Systems and were declared by the manufacturer to contain <0.1 ng of LPS per μg of protein.

Human samples

Data from 171 SLE cases consisting of patients of self-reported European ancestry that had serum available for IFN I analysis were obtained from multiple study centers. Clinical characteristics and demographic details for the patients in the replication cohort are summarized in Supplementary **Table S1**. Informed consent was obtained from all patients in both cohorts included in this study, and the study was approved by the institutional review boards at the respective institutions. Additional genotyped human PBMCs from normal donors carrying *ITGAM* non-risk or risk variant for cell based immunofluorescence and other assays were provided by the Genotype and Phenotype (GAP) Registry at the Tissue Donation Program at The Feinstein Institute for Medical Research (Manhasset, NY).

Genotyping

Patients were genotyped at coding change SNPs in ITGAM (rs1143678, rs1143679 and rs1143683) using custom designed Applied Biosystems Taqman primers and probes on an Applied Biosystems 7900HT PCR machine with >98% genotyping success. Genotyping scatter plots were all reviewed individually for quality, and genotype frequencies did not deviate significantly from the expected Hardy-Weinberg proportions (p>0.01).

Measurement of serum IFN I activity

We used an assay, which we have used extensively to measure type I IFN in human sera (4, 5). Briefly, WISH cells (ATCC #CCL-25) were cultured with 50% sera or supernatant for 6 hours and lysed. cDNA, made from cellular mRNA, was quantified using real-time PCR using forward and reverse primers for the genes interferon-induced protein with tetratricopeptide repeats 1, myxovirus resistance 1, and dsRNA-activated protein kinase (5). The PCR product of each gene was normalized to the housekeeping gene GAPDH. Fold increase in expression levels of the IFN-induced genes of cells cultured with serum samples over cells without samples was determined. Results were standardized to a healthy reference population and type I IFN activity scores were calculated based upon the mean and standard deviation (SD) of the reference population (5). The IFN assay has previously been normalized using 100 healthy controls to establish normal values for serum IFN in healthy individuals and the calculation of the IFN scores is fully described in (6). The healthy donor data were also used to establish a cutoff value for doing binary analyses with the IFN data, with high IFN being considered two SD or greater above the

mean of the healthy donor pool. This assay has been highly informative in multiple human autoimmune diseases (7-10).

Association analyses

Logistic regression analysis was used to detect associations between the individual SNPs and serum IFN I activity in this study. IFN I activity was studied as a categorical trait because the trait distribution is highly skewed, such that log transformation does not result in a normal distribution and the highly skewed data did not allow for linear modeling in a quantitative trait locus analysis. We used a binning strategy that has been highly informative in previous large scale studies and multivariate analyses of the serum IFN trait in SLE (7-10), in which subjects with a value >2 s.d. above the mean of healthy controls are binned as high IFN I, and the rest are binned as low IFN I activity. Using this binning strategy prevents high outlying values from exerting an inordinate amount of influence in the model. Logistic regression analysis was carried out using PLINK v.1.07 software. Enrichment P-values were calculated using a Fisher's exact test. Graphs were also generated showing the IFN values in patients segregated by genotype, with Mann-Whitney U test used to determine statistical significance.

Mice

The C57BL/6J (B6) wild type ((#000664, The Jackson Laboratory, Bar Harbor, ME), B6 CD11b$^{-/-}$ (#003991, The Jackson Laboratory, Bar Harbor, ME) (11), female MRL/*lpr* (#000485 The Jackson Laboratory, Bar Harbor, ME) and haplotype-, age- and sex-matched control MRL/*MpJ* (#000486, The Jackson Laboratory) were maintained in

specific-pathogen-free conditions and used in accordance with the Institutional Animal Care and Use Committee (IACUC) and the respective institutional guidelines. The MRL/*Mpj* mice were used as a non-lupus prone, haplotype-matched strain to compare lupus-prone mice to normal pathology.

SLE mouse model

Female MRL/*lpr* were treated with LA-1 (2 mg/kg/day) or vehicle (1% Tween-20 in sterile saline) for 11 weeks by daily intraperitoneal injection, beginning at 8 weeks of age until euthanasia at 19 weeks of age. Haplotype-matched female MRL/*Mpj* mice were used as phenotypic controls. The assessments were blinded for histological analysis. Sample size was chosen based on previous studies using interventions in MRL/*lpr* mice to assess similar outcomes in phenotype (12). No method of randomization was used. One mouse from the LA1 treatment group was excluded from analysis due to excessive renal pathology unrelated to lupus.

Assessment of lupus nephritis and skin involvement in mice

Serum creatinine was determined by HPLC as previously described(13), except that HPLC runs were extended from 10 min to 40 min, in order to avoid a interference from a large peak at 20-25 min. Urinary albumin and creatinine concentrations were measured using a mouse albumin ELISA (Bethyl laboratories, Montgomery, TX) and a creatinine assay (R&D systems, Minneapolis, MN), respectively. Urine albumin:creatinine ratios were then calculated. Kidneys and affected skin samples were harvested after perfusion with PBS. Regions of alopecia were measured on the face and dorsum, with greatest

diameter determined to the nearest mm with calipers. One part of the removed kidney was fixed in 10% formalin and embedded in paraffin and another part was immediately snap frozen in OCT on liquid nitrogen and stored at -80°C. Paraffin embedded sections (4 µm) were stained with hemotoxylin-eosin (H&E), periodic acid-Schiff (PAS), or Masson's trichrome. Stained slides were blindly evaluated by an experienced pathologist for chronic tubulointerstitial damage, glomerular sclerosis, and tubulointerstitial inflammation using a 0 (none), 1+ (<25%), 2+ (25-50%), 3+ (>50%) scoring system and collagen deposition was indicated as a percent of tissue area stained blue with Masson's trichrome. Formalin-fixed and frozen sections of the skin were prepared as for kidneys.

For immunofluorescence studies, tissue sections (4 µm) were cut and fixed in -20°C acetone before immunofluorescence staining. Sections were blocked (4% FBS, 4% BSA, 0.4% Fish gelatin in PBS) at room temperature for 1 hr and incubated with the appropriate primary antibodies - WT1 (2 µg/mL, SC-192, Santa Cruz), synaptopodin (2 µg/mL, SC-21537, Santa Cruz), activated β1 (5 µg/mL, 553715, BD Biosciences) or IgG (0.4 µg/mL, A11029, Thermofisher Scientific) in blocking buffer at 4°C overnight. Sections were incubated with the appropriate secondary antibody (Thermofisher Scientific) and mounted with DAPI medium (Vector Laboratories). Fluorescence images were acquired using a Zeiss LSM 700 confocal microscope with a PLAN-Apochromat 20x objective and an AxioCam camera and analyzed using the Zen software (Carl Zeiss Group). The number of WT1 positive cells per glomeruli was calculated manually using the confocal microscope (5 glomeruli/tissue). The fluorescence intensities for

synaptopodin, activated β1, and IgG were calculated using the ImageJ Software (5-8 glomeruli/tissue).

Serum quantification of autoantibodies and total IgG

Commercial ELISAs for murine anti-dsDNA antibodies and total IgG were purchased from Alpha Diagnostic (San Antonio, TX, catalog# 5110 and 6320, respectively) and were performed according to the manufacturer's instructions in serum obtained at 19 weeks of age.

Murine bone marrow isolation

Cells were isolated from the bone marrow by flushing the femurs and tibias with HBSS with 15 mM EDTA. The cells were then spun on a 52%, 69%, 78% Percoll gradient at 1500 g for 30 minutes. Cells were collected from the 69%-78% interface and then spun down, resuspended in RBC Lysis Buffer (eBioscience) and washed before being resuspended in RPMI-1640.

Murine monocyte isolation

Isolation of mouse bone marrow or spleen monocytes was performed using the EasySep Mouse Monocyte Enrichment Kit (Cat#19761, Stemcell) according to the manufacturer's instruction.

Flow cytometry of mouse splenocytes for immunophenotyping

A single cell suspension of mouse splenocytes was prepared using a cell strainer, rinsing with FACS buffer. The cells were washed with PBS and then underwent RBC lysis using 1x multi-species RBC Lysis Buffer (Cat#00-4333-57, eBioscience). The cells were washed again in PBS and resuspended in FACS buffer (2% FBS in PBS) at 1.0×10^6 cells/mL for analysis by flow cytometry. After blocking for 15 minutes, cells were resuspended in 100uL FACS buffer and incubated with 2uL each of respective antibodies or isotype control for 30 minutes, fixed with 2% paraformaldehyde, quantified by flow cytometry using a BD FACSCanto RUO and data analyzed using FlowJo Software. Cutoff values for positive staining were determined using compensation controls for each fluorophore. All antibodies were from Biolegend (San Diego, CA): Alexa Fluor 488®-anti-mouse CD3 antibody (clone 17A2), PE-anti-mouse CD4 antibody (clone GK1.5); APC-anti-mouse CD8 antibody (clone 53-6.7); PE Cy/7-anti-mouse CD11c antibody (clone N418); Alexa Fluor 488-anti-mouse CD19 antibody (clone 6D5); PE Cy/7-anti-mouse CD25 antibody (clone PC61); PerCP/Cy5.5-anti-mouse CD69 antibody (clone H1.2F3); PE-anti-mouse CD80 antibody (clone16-10A1); PerCP/Cy5.5-anti-mouse CD138 antibody (clone 281-2); Pacific Blue™-anti-mouse B220 antibody (clone RA3-6B2); APC/Cy7-anti-mouse F4/80 antibody (clone BM8);FITC anti-mouse Ly6G antibody (clone 1A8). Results are reported as number of cell subsets/million splenocytes.

Cecal ligation and puncture model

Cecal ligation and puncture (CLP) was performed as described previously (14) using B6 WT mice (8-12 weeks old). Vehicle control (1% DMSO in PBS) or LA1 (2mg/kg body weight, in PBS) was administered *intraperitoneally* 2 hrs prior to CLP and then daily

until the end of the experiment. No mice were excluded from analysis and no method of randomization was used. Sample size was chosen based on previous studies to assess similar outcomes (14). For the colony-forming units assay, blood samples from septic or mock CLP mice were collected by cardiac puncture at indicated times after surgery. Mice were subsequently perfused *in toto* with 10mL ice cold PBS and spleen, liver and kidneys were surgically removed and homogenized in 5ml of sterile PBS. Serial dilutions of blood and tissue homogenates were immediately plated on Trypticase Soy Agar II plates supplemented with 5% Sheep Blood. CFUs were counted after 12h of incubation at 37°C. The serology and cytokine measurements were performed as described (14) using plasma from blood samples obtained 24 hours post-CLP. LDH, CK, ALT and urea levels were measured using the BioAssay Systems kits (BioAssay Systems, California) according to company's protocol. Levels of IL-1β, IL-6 and TNFα were measured using the murine ELISA kits (R&D Systems, Minneapolis) according to company's protocol.

In vivo viral infection assay

H1N1 infection and viral particle quantification was performed using B6 WT mice as previously described (15). Infection was performed by intranasal application of virus solution in 20 µl of sterile phosphate-buffered saline under light isofluorane anaesthesia. Un-infected wild-type B6 WT mice were included as controls. Sample size was chosen based on previous studies to assess similar outcomes. Body weight loss was monitored until day 14 p.i.

LPS Mouse Model

The endotoxin shock model using LPS administration in 8-12 wk old B6 WT and CD11b $^{-/-}$ mice was performed according to literature protocols (16). Briefly, LPS (*E. coli* strain O111:B4, Invivogen) was administered by *intraperitoneal* injection (15mg/kg) in mice. Vehicle control (1% DMSO in PBS) or LA1 (2mg/kg body weight, in PBS) was administered *intraperitoneally* 30 min after the LPS injection and the animals were sacrificed after 4h and sera was collected. Mice injected with vehicle (1% DMSO in PBS) alone were used as controls (C). No mice were excluded from analysis and no method of randomization was used. Sample size was chosen based on published studies (16). IFNβ level in the sera was measured using the murine ELISA kits (PBL Assay Science, Piscataway, NJ, catalog# 42400-1) according to company's protocol.

Vascular re-endothelialization in rats

The wild type Fischer 344 rats were purchased from Harlan Laboratories (Indianapolis, IN). Vascular healing was evaluated after balloon induced arterial injury. All operative procedures were under isoflurane anesthesia (Baxter, IL, USA). The endothelium of the right iliac artery of male Fisher rats (280-320 grams) was removed using a 2F Fogarty catheter (Baxter Corp., Irvine, CA, USA) adapted to a custom angiographic kit (Boston Scientific, Scimed) (17). Rats received daily peritoneal injections of LA1 or vehicle. Seven days post-surgery, 0.5 mL of 5% Evans blue was injected into the tail vein of treated and control animals 30 min before euthanasia, and perfusion-fixation with 4% phosphate-buffered paraformaldehyde were performed. The injured arterial segment was dissected and mounted on a microscopic glass slide. The blue-stained area, denuded area was measured with the Image Pro Plus software (Media Cybernetics). Alternatively,

injured segments were immersed in 1 ml of N,N-dimethyl formamide (Sigma, St. Louis, Mo.) for 48 h to extract the Evans blue dye. The absorbance of Evans blue dye solution was measured in a spectrophotometer at 630 nm. The re-endothelialization was further confirmed using immunohistochemistry (18) with a rabbit anti-human Von-Willebrand factor antibody (DAKO, 1:400) after paraffin-embedding and cross sectioning of all injured vessels. Morphometric analysis was performed in a blinded fashion using NIH ImageJ.

Cell lines

The cell lines HEK 293T, K562 and RAW murine macrophage were all obtained from the American Type Culture Collection (ATCC) and were maintained accordingly. K562 cells stably transfected with integrin CD11b/CD18 (K562 CD11b/CD18) using the pcDNA3 plasmids encoding CD18 wild type and either CD11b wild type (WT), mutant CD11bE320A (E320A), CD11bI316G (I316G) or CD11bR77H (R77H) were prepared as described previously (19, 20). The pcDNA3 CD11bR77H plasmid was a gift from S. Fagerholm (University of Helsinki, Helsinki, Finland) (20). Cell lines were tested and determined to be mycoplasma free.

Cell adhesion assays

Cell-based adhesion assays with immobilized Fg as ligand were performed as previously described (19). A stock solution of LA1 was prepared in DMSO at a concentration of 10 mM. The final concentration of DMSO in the assay wells was approximately 2%. Assays

were performed in 3 to 6 replicate wells. Data shown are from one of at least three independent experiments.

Isolation of human monocytes and differentiation into primary macrophages

Human peripheral blood mononuclear cells (PBMCs) were isolated from fresh blood collected from healthy volunteers under an IRB-approved protocol and using RosetteSep (human monocyte Enrichment Cocktail, Cat# 15068 Stemcell Technologies, Vancouver, Canada) followed by Ficoll-Hypaque density gradient centrifugation according to published protocols[21]. The cells were washed, resuspended in RPMI1640 with GlutaMAX (Cat# 61870-036, GIBCO) and autologous human serum (5%) (complete medium), and seeded into T75 (75 cm^2) tissue culture flask (Cat#156800, Thermo). Non-adherent cells were removed by gentle pipette aspiration after 2 h of incubation at 37°C in a humidified atmosphere containing 5% CO^2. Subsequently, an equal volume of fresh complete medium was added to each flask and the cells were placed back in the incubator for approx. 24h. Subsequently, adherent cells were washed twice with PBS, detached from the flask by scraping with a rubber policeman, stained with trypan blue dye and counted using a hemocytometer. The cells (≥85% monocytes as determined by flow cytometric analysis after staining with anti-CD14 mAbs) were seeded in 6-well tissue culture dished (Cat #353847, Corning) at a density of 2×10^6 cells/well and were cultured for 5-7 additional days at 37°C in 5% CO_2 to promote their full differentiation into monocyte-derived macrophages (22, 23).

Isolation of murine primary neutrophils and macrophages

Thioglycollate-elicited neutrophils and macrophages were isolated from B6 WT mice or B6 CD11b^{-/-} mice, as described previously (19). Neutrophils were collected 4h after thioglycollate injection followed by 1h adherence purification before collecting non-adherent cells. The macrophages were collected four days post thioglycollate injection and adherence purified for 1h, followed by a wash with PBS to remove non-adherent cells. For the bone marrow derived macrophages (BMM), 2×10^6 cells/well of harvested cells were plated in 6-well plates in RPMI containing 10% FBS and were cultured for 5-7 days. Macrophages were generated from bone marrow derived monocytes cells as described in the literature (24).

Microarray analysis

Human macrophages (2×10^6) were cultured in 6-well tissue culture plates and were treated with LPS (50ng/mL) in the absence or presence of LA1 (20μM) for 4h as previously described (19). Cells were washed with ice cold PBS and the lysed in TRIzol (Thermo Fisher Scientific, Waltham, MA) for total RNA isolation. RNA sample quality was analyzed using a 2100 Bioanalyzer (Agilent). Whole genome transcriptional profiling was performed at the University of Chicago Genomics Core using Illumina HT-12 human gene expression arrays. The raw data from microarray analyses was uploaded on GeneSpring™ software v13. Quality control steps were performed and data was Quantile normalized and $\log_2$ transformed to mean of all samples. Significance test was performed using the unpaired Student's t-test and p-values were multiple testing corrected using the Benjamini-Hochberg method. Only significant genes (p-value <= 0.05 and fold change >= 2) were considered for pathway analysis. We deposited all

microarray data in the Gene Expression Omnibus database in the series GSE76802. We generated hierarchical clustering graphs on normalized gene expression fold change with respect to the mean expression value using Plotly.

Pathway analysis

Significantly different genes between two conditions were loaded on GeneGO™ web portal from Thomson Reuters. Significantly enriched pathways (p-values < 0.05) were generated and analyzed on the portal.

mRNA quantification in human macrophages using nCounter

Human macrophages were stimulated with LPS (50ng/mL) for various amount of time (0, 0.5, 2, 4, 8 and 24h) in the absence or presence of LA1 (20µM) as described previously (19). Total RNA was extracted using TRIZOL reagent and QIAGEN's total RNA isolation kit according to manufacturer's instructions. RNA sample quality was analyzed using a 2100 Bioanalyzer (Agilent). Expression levels of selected genes were measured using an inflammation panel set and the nCounter Digital Analyzer (Nanostring Technologies, Seattle, WA) as previously described (25) and following the manufacturer's instructions at the University of Miami Genomics Core. Data analysis was performed as described (25) after normalization using internal Nanostring controls (spike-normalization following manufacturer's instructions).

Quantification of IFN I-inducible genes and FOXO3 in murine cells

RNA isolation and real-time PCR for quantification of IFN I–inducible genes were performed as described previously. Briefly, RNA was isolated from spleens and bone marrow using TriPure Isolation Reagent (Roche) according to the manufacturer's instructions. cDNA was synthesized using MMLV RT (Invitrogen) and 1 µg of RNA using a MyCycler Thermocyler (Bio-Rad). Five IFN I–responsive genes and 1 housekeeping gene (β-actin) were quantified by real-time PCR using SYBR Green PCR Supermix (BIO RAD, USA) according to the manufacturer's instructions. The primer sequences for the *Mx1*, *Irf7*, *Ip-10*, *Isg15*, and *Ifng* genes have been described by our group previously and are as follows:

mIRF7_F	TGC TGT TTG GAG ACT GGC TAT
mIRF7_R	TCC AAG CTC CCG GCT AAG T
mMCP1_F	AGG TCC CTG TCA TGC TTC TG
mMCP1_R	TCT GGA CCC ATT CCT TCT TG
mISG15_F	CAG AAG CAG ACT CCT TAA TTC
mISG15_R	AGA CCT CAT ATA TGT TGC TGT G
mIFNg_F	ATG GCT AGR CTC TGT GCT TTC CT
mIFNg_R	AGG GCT CTC CAG AYT TCT GCT CTG

For quantification of murine FOXO3 mRNA levels, RNA from splenic monocytes was isolated using Direct-Zol RNA MiniPrep Plus (Cat#R2072, Zymo Research). cDNA was synthesized with 500 ng of RNA using BioRad 5x iScript Reverse Transcription Supermix (Cat#170-8841, Bio-Rad) using a Veriti 96-Well Thermal Cycler (Applied Biosystems). *Foxo3* and the house-keeping gene *β–actin* were quantified by real-time

PCR using the SsoAdvanced Universal SYBR Green SuperMix (Cat#1725274, Bio-Rad). The primer sequences for *Foxo3* and *β-actin* are listed below, and real-time PCR was carried out using the C1000 Touch Thermo Cycler (Bio-Rad). The transcripts were normalized using β-actin gene. The data was presented as fold change based on the formula $2^{-\Delta\Delta Ct}$.

mFoxo3_F	AAC AGA CCA GCC ACC TTC TCT T
mFoxo3_R	TGA AGC AAG CAG GTC TTG GA
mβ-Actin_F	CCA ACC GCG AGA AGA TGA
mβ-Actin_R	CCA GAG GCG TAC AGG GAT AG

Quantification of IFN I pathway genes in human PBMCs

Total RNA was isolated from human PBMCs using QIAzol Reagent (Life Technologies) and Qiagen RNA isolation kit according to the manufacturer's instructions. cDNA was synthesized using High Capacity cDNA Archive Kit (Life Technologies) and the resulting cDNA samples were subject to real-time quantitative reverse-transcription polymerase chain reaction (qRT-PCR) analysis with CFX96^{TM} Real-Time System (Bio-Rad). qRT-PCR was run in a 20-μL reaction using TaqMan Gene Expression Master Mix (Applied Biosystems) according to the manufacturer's instructions. Briefly, qRT-PCR was performed (40 cycles of 95 °C for 15 s and 60 °C for 1 min) and the resulting cycle threshold (Ct) values of individual genes were normalized to Ct values for human GAPDH (ΔCt), and then were used to calculate fold change in relative gene expression ($2^{-\Delta\Delta CT}$). All samples were run in at least duplicates. The predesigned TaqMan gene

expression assays for human *IFNB1* (Hs01077958_s1), *IRF7* (Hs01014809_g1), and *GAPDH* (Hs02758991_g1) were purchased from Thermo Fisher Scientific.

Luminex analysis of serum cytokine samples

The concentrations of mouse serum cytokines were determined using the cytokine mouse 20-plex panel for Luminex platform (Invitrogen/ThermoFisher Scientific) according to the manufacturer's protocols. The concentrations of cytokines were calculated according to the standards for each assay.

ELISA assays

Primary human and mouse macrophages were cultured in the presence of vehicle (1% DMSO), LA1 (20 μM), LPS (50ng/mL), or LPS (50ng/mL) and LA1 (20 μM) for various time points (4h, 8h, 12h) and the cell culture supernatant was collected. Human cell culture supernatants were assayed using a sandwich ELISA kits for human IL6 (R&D Systems, Minneapolis, MN, catalog# D6050), IL-1β (R&D Systems, Minneapolis, MN, catalog# DLB50), TNF-α (R&D Systems, Minneapolis, MN, catalog# DTA00C) and MCP-1 (R&D Systems, Minneapolis, MN, catalog# DCP00) according to manufacturer's instructions. Mouse cell culture supernatants were assayed using commercially available sandwich ELISA kits for mouse IL6 (R&D Systems, Minneapolis, MN, catalog# M6000B), IL-1β (R&D Systems, Minneapolis, MN, catalog# MLB00C), and TNF-α (R&D Systems, Minneapolis, MN, catalog# MTA00B) according to manufacturer provided instructions. For measuring IFNβ levels, mouse macrophages (WT and CD11b$^{-/-}$) were cultured in the presence of vehicle (1% DMSO), LA1 (20 μM), LPS (100ng/mL),

or LPS (100ng/mL) and LA1 (20 µM) for 12h and the cell culture supernatant were assayed using commercially available sandwich ELISA kits for mouse IFNβ (PBL Assay Science, Piscataway, NJ, catalog# 42400-1) according to manufacturer provided instructions.

Western blot

RAW macrophages were cultured in the presence of vehicle (1% DMSO), LA1 (20 µM), LPS (50ng/mL), or LPS (50ng/mL) and LA1 (20 µM), or pI:C (25µg/mL), or pI:C (25µg/mL) and LA1 (20 µM), for various durations (0, 30, 60, 120 and 240 min). Human and mouse primary macrophages were similarly treated. The cells were washed with ice cold PBS and were subsequently lysed in Laemmli buffer (120mM Tris-HCl pH 6.8, 4% w/v SDS, 20% glycerol, 1% β-mercaptoethanol) along with protease inhibitor cocktail (Roche Applied Science, Indianapolis, IN Cat# 11836153001) and phosphatase inhibitor cocktail (Thermo Scientific, Rockford, IL, Cat# 88667) for 30 minutes at 4°C. Nucleic acid was sheared by passing through 28.5 gauge syringe 5 to 10 times. Lysate was cleared by centrifugation at 16,000 xg for 10 min at 4°C. Protein concentration was determined using the BCA Protein Assay (Pierce, Rockford, IL). Equal amount of proteins were separated on a 4-12% gradient NuPAGE Bis-Tris Gel (Invitrogen) and blotted to a PVDF membrane (Millipore). Membrane was blocked with 10% BSA for 1 hr at RT, followed by incubation with various primary antibodies overnight at 4°C. Subsequently, membrane was washed and incubated with either HRP conjugated goat anti-mouse or anti-rabbit for 1 hour at RT and detected using chemiluminescent substrate (Cat# 34080, Thermo Scientific, Waltham MA). Membranes were stripped with Restore

18

stripping buffer (cat#21059 Thermo Scientific, Pierce, Rockford, IL), and reprobed with anti-GAPDH antibody (cat# 2118, Cell Signaling) and developed as mentioned above. Data presented is representative of at least three independent experiments.

For quantification of FOXO3 protein in murine bone marrow monocytes from lupus mice, the isolated cells were lysed with 50mM Tris-HCl pH 7.4, 300 mM NaCl, 0.5% w/v Triton X-100, 5mM EDTA, protease inhibitor cocktail (Roche Applied Science, Indianapolis, IN) for 30 minutes at 4° C. Lysate was cleared by centrifugation at 16,000 xg for 10 min at 4° C. Protein concentration was determined using the BCA Protein Assay (Pierce, Rockford, IL). Equal amounts of protein were separated on a 4-12% gradient NuPAGE Bis-Tris Gel (Invitrogen) and blotted to a PVDF membrane. Membrane was blocked with 10% BSA for 30 min at RT, followed by incubation with either anti-total FOXO3a (75D8) (Cell Signaling) or anti-phospho FOXO3a (S253) (Cell Signaling) overnight at 4°C. Subsequently, membrane was washed and developed as mentioned above. Data presented is representative of at least three independent experiments.

Assessment of endothelium-dependent vasorelaxation

After euthanasia, thoracic aortas were excised, cleaned, and cut into 2-mm length rings. Endothelium was left intact, and aortic rings were mounted in a myograph system (Danish Myo Technology A/S). Vessels were pre-contracted with PSS containing 100 mM potassium chloride (KPSS) and then returned to PSS. Cumulative concentrations of PE (10^{-9} M to 10^{-6} M) were then added to the bath to establish a concentration-response

curve. A PE concentration corresponding to 80% maximum was added, and contraction was allowed to reach a stable plateau. To examine endothelium-dependent relaxation, Acetylcholine (Ach, 10^{-9} M to 10^{-6} M) was added cumulatively to the bath and a curve was generated. Finally, a normal vascular smooth muscle response was confirmed by removing PE and Ach.

Expression and purification of recombinant CD11bA

The recombinant human CD11bA (CD11bA) spanning residues Gly111-Gly321 was obtained as previously described (19). Briefly, the CD11bA domain in pGEX-2T was expressed as glutathione S-transferase (GST) fusion protein in *Escherichia coli* and purified by affinity chromatography (Glutathione-beads, Sigma) following manufacturer's instructions. The GST-tag was removed using TEV protease to release CD11bA, which was further purified using Fast Protein Liquid Chromatography (FPLC, AKTA purifier) with a Source S column and eluted with a NaCl gradient (0-0.5M) in 20 mM Tris-HCl, pH 8.0. The purity of CD11bA was confirmed by 1D SDS-polyacrylamide gel electrophoresis analysis. Purified CD11bA was dialyzed against 20 mM Tris-HCl, pH 7.5, 150 mm NaCl and subsequently used in ITC assays.

Isothermal titration calorimetry (ITC)

ITC experiments were performed using published protocols (26) using a MicroCal ITC$_{200}$ microcalorimeter (GE healthcare) with a reaction cell volume of 200 μl and syringe volume of 40 μL. Briefly, the heat flow resulting from the binding of LA1 to CD11bA in the absence or presence of various metal ions (Mn^{2+}, Ca^{2+} and Mg^{2+}) was measured at

25 °C (298 K) with high sensitivity. LA1 (5μM) in reaction buffer (0.2% DMSO in Tris buffered saline (TBS)) was placed in the calorimeter reaction cell and stirred at 1000 rpm. CD11bA (70μM) was placed in the calorimeter syringe in the same reaction buffer and in the absence or presence of various metal ions (1mM each). The protein was injected in a step-wise fashion into the reaction cell with an injection volume of 2.5μL, with duration of 4s. Interval between injections was 60s. In another set of experiments, CD11bA (20μM) was placed in the calorimeter reaction cell in the absence or presence of LA1 (5μM). The solution in the cell was titrated with concentrated metal ions (Mn^{2+}, Ca^{2+} and Mg^{2+}) filled in the calorimeter syringe. The reaction buffer, injection volume, duration and interval between the injections were as above. The heat flows from control experiments (injection of protein into reaction cell containing only the reaction buffer) were also measured and were subtracted from the heats measured for each of the binding reactions. Data were analyzed and fitted using the Microcal Origin software provided with the instrument. The experimental data were fitted to a model for simple binding of LA1 to a single class of sites (n=1) on the protein CD11bA. The enthalpy of binding, ΔH (kcal/degree/mol), was determined from the heat release measurement, which is independent of the binding model.

Computational modeling and molecular dynamics simulations

We employed a multistep computational strategy to investigate the interactions of LA1 with CD11bA. In the first step, published X-ray structures of CD11bA (27, 28) were used to build LA1 docked computational models, as previously described (19). Structures were equilibrated using all-atom 30 ns molecular dynamics (MD) simulations in an aqueous

solution using the GROMACS program (29, 30) and the OPLS-AA (Optimized Potentials for Liquid Simulations) force field (31). In the simulations, the starting structures were placed in a large cubic box (60.0 x 60.0 x 60.0 Å^3) to avoid artificial interactions with their images in the neighboring boxes created by the application of periodic boundary conditions. The box was filled with TIP3P water molecules. Some water molecules were replaced with sodium and chloride ions to neutralize these systems and to simulate an experimentally used ion concentration of 150mM. The starting structures were subsequently energy-minimized with a steepest descent method for 3000 steps. The results of these minimizations produced the starting structure for the MD simulations. The MD simulations were then carried out with a constant number of particles (N), pressure (P) and temperature (T), *i.e.*; NPT ensemble. The SETTLE algorithm was used to constrain the bond length and angle of the water molecules (32), while the LINCS algorithm was used to constrain the bond length of the protein (33). The long-range electrostatic interactions were calculated by the Particle-Mesh Ewald (PME) method (34). A constant pressure of 1 bar was applied with a coupling constant of 1.0 ps peptide, water molecules and ions were coupled separately to a bath at 300 K with a coupling constant of 0.1 ps. The equation of motion was integrated at each 2 fs time steps using leap-frog algorithm (35). The tools available in the GROMACS program package and the YASARA software (v.13.2.2) were utilized for analyzing trajectories and simulated structures (36). The most representative structure provided by these simulations was subsequently used to study CD11bA-LA1 interactions. The most representative structures were derived from cluster analysis, where the trajectories were analyzed by grouping structurally similar frames (root-mean-square deviation cutoff = 0.30 nm) (37), and the

frame with the largest number of neighbors was denoted as a middle structure that represented that particular cluster. In the next step, a LA1 molecule was docked inside the cavity of CD11bA using the Autodock Vina 1.1.2 software (38). In these docking experiments the protein was kept rigid, but the LA1 molecule had the flexibility to adopt different conformations. In the next step, the most promising poses provided by the docking procedure were subjected to 30 ns all-atom MD simulations in an aqueous solution. These simulations were also performed using GROMACS (29, 30) and GROMOS96 53A6 (39). The secondary structure analyses were performed by employing the defined secondary structures of proteins (DSSP) protocol (40). The RMSD of all trajectories indicated that they were well equilibrated within the 30 ns time frame.

Flow chamber assay

The flow chamber assay was performed as described (41). A polystyrene Petri dish was prepared by coating with a 5 mm diameter, 20 μL spot of 20 μg/mL purified h-ICAM-1/Fc or 20 μg/mL Fibrinogen in coating buffer (PBS, 10 mM NaHCO$_3$, pH 9.0) for 1 hr at 37°C, followed by blocking with 2% BSA in coating buffer for 1 hr at 37°C. HEK 293T cells were transiently transfected with CD11b WT and CD18 WT plasmids (WT), CD11bE320A and CD18 WT (E320A), or CD11bI316G and CD18 WT (I316G) as previously described (42). The transfected HEK 293T cells were washed twice with wash buffer (20 mM HEPES, 150 mM NaCl, pH 7.4, 5 mM EDTA/0.5% BSA) and, subsequently, once with HEPES buffered saline (HBS) containing 1 mM Ca^{2+} and 1mM Mg^{2+} (HBS^{++}). The cells were resuspended at the concentration of 5x10^6/mL in HBS^{++} (Ca^{2+} and Mg^{2+}-free HBS, 0.5% BSA) and kept on ice. Cells were incubated with LA1

(25 µM) or vehicle (2% DMSO) for 30 min at 37°C prior to infusion in the flow chamber using a Harvard apparatus programmable syringe pump. Upon infusion, the cells were allowed to settle down for 5 min, and accumulate for 30 sec at a shear stress of 0.3 dyn/cm^2 and 10 sec at 0.4 dyn/cm^2. Subsequently, shear stress was increased every 10 sec from 1 dyn/cm^2 up to 32 dyn/cm^2, in 2-fold increments. The number of cells remaining abound at the end of each 10-sec interval was determined by manual counting. Rolling velocity at each shear stress was calculated from the average distance traveled by rolling cells in 3 sec. Rolling adherent cells were defined as cells moving with a velocity of more than 1 µm/s.

Immunofluorescence

Sub-cellular localization of FOXO3 and NFkB in primary macrophages and in RAW cells was quantified as described (43). Briefly, cells ($1X10^4$ to $5X10^4$) were plated on poly-L-lysine-coated MatTek glass-bottom dishes (MatTek Corporation, Ashland, MA) and were treated with vehicle (1% DMSO) (C), LA1 (20 µM), LPS (50 ng/mL), or LPS (50ng/mL) and LA1 (20 µM) for 4h. The cells were fixed (4% paraformaldehyde in PBS), blocked (5% normal goat serum in PBS), permeabilized (with 0.1% Triton X-100), and stained with either anti-FOXO3a (cat# 2497, Cell Signaling) or anti-p65 (NFkB) (cat# 16502, Abcam) antibodies. Subsequently, the cells were washed and stained with AlexaFluor568-conjugated secondary antibody (Cat# A11011, Life technologies). Nuclear staining was performed using DAPI dye. Images were captured on a Zeiss LSM 700 Confocal Microscope and analyzed in a blinded fashion with NIH ImageJ software.

Apoptosis assays

Apoptosis was evaluated by TUNEL using TACS 2TdT-Fluor Apoptosis detection kit (cat# 4812-30-K, TREVIGEN) as per manufacturer's assay protocol where nicked DNA was used as positive control and nuclear staining was performed using DAPI. Apoptosis was also evaluated as a measure of Lactate dehydrogenase (LDH) release by the cells using LDH cytotoxicity assay kit (cat# 601170, Cayman chemical, MI) according to the manufacturer's protocol.

Statistical analysis

To calculate statistical significance, a two-tailed student's *t*-test was used, unless otherwise specified. The differences in the cytokines concentrations were statistically analyzed using the Mann-Whitney test, and plotted with GraphPad Prism software package. For multiple comparisons, one-way ANOVA with Tukey's test was used. A value of $P < 0.05$ was considered statistically significant. For endothelium-dependent vasorelaxation, curves were first analyzed using an asymmetric (five parameters) logistic equation, and significance of each individual data point was determined by two-way ANOVA. Unless otherwise specified, results are represented as mean ± SEM.

Supplemental Text

LA1 partially activates CD11bA to an intermediate affinity conformation

We previously showed that CD11b agonist LA1 binds to the ligand-binding domain of CD11b (CD11bA-domain) (Fig. S2C) and allosterically enhances ligand binding of both full-length CD11b/CD18 and the isolated, recombinant CD11bA (19). Studies using conformation-specific antibodies showed that LA1 does not induce large conformational changes in the integrin heterodimer (44). To gain additional molecular insights, we utilized molecular dynamics studies using published structures of CD11bA, as well as a model of LA1 docked into CD11bA (19, 45). Results (Figs. S2D-S2G), shown as a superposition of CD11bA in closed (yellow), open (red) and energy minimized LA1-docked structure (red), suggest that the LA1 bound structure adopts a partially active, intermediate affinity conformation (46), where the F-α7 loop, α7 helix and the α1 helix showed structural shift halfway between the closed and the open conformation, thereby priming the integrin (Fig. S2G). To confirm, we used isothermal titration calorimetry (ITC) to directly assess the binding of LA1 with CD11bA. We measured the heat flow in the absence or presence of various metal ions (Mn^{2+}, Ca^{2+} and Mg^{2+}). In the absence of LA1, the observed thermodynamic data for the interaction of three metal ions with CD11bA was similar to the data reported in literature (26) (Table S2). However, a dramatic favorable enthalpy-driven increase in the binding affinity of all three metal ions was observed in the presence of LA1 with CD11bA (Fig. S3A), which suggests that LA1 creates a favorable environment for binding of metal ions. Next, the heat flow was measured by placing LA1 in the cell and titrating it with a solution of CD11bA bound to various metal ions. LA1 showed no binding to the metal ions alone.

Fitting the experimental data to a model for simple binding of LA1 to a single class of sites (n=1) on the protein displayed almost no LA1 binding to CD11bA in the absence of metal ions (Fig. S3B), but showed a 45-fold increase in the affinity of LA1 to CD11bA in the presence of all three metal ions which is largely driven by favorable enthalpy (Table S3). These data confirm direct LA1 binding to CD11bA, where its affinity for CD11bA is modulated by metal ions.

In vivo, circulating leukocytes adhere to the surface of inflamed endothelium under fluid shear stress. To examine the strength of LA1-stimulated adhesion of CD11b/CD18 to immobilized ligands, human ICAM-1–IgG$_1$ Fc fusion protein (ICAM-1) or fibrinogen (Fg), we utilized a parallel plate shear flow adhesion assay (41). CD11b/CD18-expressing cells (WT) were allowed to accumulate on the immobilized ligands at a wall shear stress of 0.3 dyne·cm^{-2} for 30s. Subsequently, the wall shear stress was incrementally increased every 10s, and the velocity of the cells that remained bound at each increment was determined and used to quantify the rolling and firmly adherent cells. We found that, as compared to the adhesion under control physiologic buffer condition (Ca^{2+} and Mg^{2+}, 1mM each) activation using the known integrin agonist Mn^{2+} (1mM) significantly increased the number of firmly adherent WT cells at the initial 0.3 dyne·cm^{-2} shear stress (Figs. S4A-S4B). LA1 treatment increased the number of both rolling and firmly adherent cells, as compared to the control. However, LA1-mediated increase in firmly adhered cells was significantly lower than the cells activated with Mn^{2+}, suggesting that LA1 may not fully activate the integrin. Moreover, under increasing shear stress conditions (Fig. S4C), the adhesive behavior of LA1-activated cells was halfway between that of the control condition (where low affinity integrin conformation primarily

mediates weak, rolling adhesion) and the Mn^{2+} activation condition (where high affinity conformation mediates firm adhesion that resists high shear stress), and greatly mimicked the behavior of integrins in an intermediate conformation (46). This further indicates that LA1 binding *per se* induces integrin priming or intermediate conformation, rather than full activation.

The I316G substitution in CD11b constitutively activates the integrin heterodimer. Conversely, the E320A substitution in CD11b suppresses integrin activation, by de-linking the CD11bA domain from the rest of the integrin chain. LA1, by binding to the CD11bA and inducing a conformational switch, is able to rescue ligand binding by the E320A mutant integrin (19). We utilized these two integrin mutants to further investigate the effects of LA1 on CD11b/CD18 activation. We found that under basal conditions, I316G expressing cells showed high firm adhesion to the two ligands (ICAM-1 and Fg), whereas both the WT and the E320A mutant expressing cells showed little binding (Figs. S4C-S4E). Activation with agonist Mn^{2+} ions slightly increased the level of adhesion by I316G expressing cells, but dramatically enhanced both firm and rolling adhesion by the WT cells. As has been shown before, Mn^{2+} did not increase binding by the E320A cells. As shown above, LA1 treatment of WT cells primarily induced rolling adhesion. Surprisingly, LA1 also dramatically increased the number of I316G cells showing rolling adhesion. Similarly, it significantly enhanced binding of E320A cells, primarily via rolling adhesion. In sum, these data establish that LA1 induces partial integrin activation and an intermediate affinity conformation in CD11bA.

CD11b activation via LA1 does not harm the vascular endothelium

Inflammatory activation of the vascular endothelium upregulates expression of β2 integrin ligands (such as ICAM-1) on cellular surface that leads to increased leukocyte adhesion and typically results in endothelial cell damage due to the release of highly cytotoxic reactive oxygen species (ROS) and proteases by the adherent neutrophils. Therefore, a key concern with the development of therapeutics using integrin activation as a mechanism of action has been whether the subsequent enhancement in neutrophil (and other leukocyte) cell adhesion would lead to increased localized damage of the endothelium. To address this issue, we performed two sets of experiments. *One*, we used an arterial balloon injury model to determine local effects of LA1 treatment on endothelial injury *in vivo*. As previously reported, LA1 reduces neointimal hyperplasia in a dose-dependent fashion post balloon angioplasty (19, 44). We examined vascular re-endothelialization in balloon-injured Fisher male rats treated with either LA1 or vehicle. Endothelial damage was measured using Evan's blue vital staining, where the denuded vascular regions show blue staining due to high permeability of the albumin-bound Evan's Blue dye, whereas intact endothelium does not (47). Seven days after balloon angioplasty, arteries from control animals showed high blue staining (Fig. 6B), whereas, minimal blue staining was observed in injured arteries of LA1-treated rats. Quantification showed a significantly reduced uptake of the Evan's blue dye by LA1 treated arteries (Fig. 6C). Immunohistochemical staining with anti-von Willebrand factor (vWF) antibody, which stains the vascular endothelium (48), showed significant re-endothelialization at the site of balloon injury with LA1 treatment (Fig. 6D), suggesting that LA1 may accelerate the process of endothelial regeneration (49). Additionally, we analyzed

animals that received a high dose of LA1 (2mg/kg/d for three weeks) and did not observe any signs of systemic vascular injury or leakage, edema or systemic vascular compromise in the liver, spleen, kidney, lung and heart (not shown), mitigating the concern of systemic vascular toxicity of LA1. *Two*, we co-incubated neutrophils with human vein endothelial cells (HUVECs) *in vitro* in the absence or presence of LA1 and measured HUVEC cytotoxicity. We did not observe increases in DNA damage (Fig. S14A-S14B) or apoptosis (Fig. S14C) in the HUVEC monolayer incubated with neutrophils in the presence of LA1 over untreated, control cells. Together, these results show that LA1 treatment does not harm the endothelium. Similarly, previously studies by others using knock-in animals that express constitutively active mutants of integrins CD11a/CD18 (50, 51) or α4β7 (52) have not reported any signs of vascular injury in the various experimental models, suggesting that integrin activation, *per se,* may not harm the vasculature or have any harmful consequences for animals under normal conditions.

Supplemental References

1.   Arnaout, M.A., Todd, R.F., 3rd, Dana, N., Melamed, J., Schlossman, S.F., and Colten, H.R. 1983. Inhibition of phagocytosis of complement C3- or immunoglobulin G-coated particles and of C3bi binding by monoclonal antibodies to a monocyte-granulocyte membrane glycoprotein (Mol). *J Clin Invest* 72:171-179.

2.   Wright, S.D., Rao, P.E., Van Voorhis, W.C., Craigmyle, L.S., Iida, K., Talle, M.A., Westberg, E.F., Goldstein, G., and Silverstein, S.C. 1983. Identification of the C3bi receptor of human monocytes and macrophages by using monoclonal antibodies. *Proc Natl Acad Sci U S A* 80:5699-5703.

3.   Springer, T., Galfre, G., Secher, D.S., and Milstein, C. 1979. Mac-1: a macrophage differentiation antigen identified by monoclonal antibody. *Eur J Immunol* 9:301-306.

4.   Hua, J., Kirou, K., Lee, C., and Crow, M.K. 2006. Functional assay of type I interferon in systemic lupus erythematosus plasma and association with anti-RNA binding protein autoantibodies. *Arthritis Rheum* 54:1906-1916.

5.   Niewold, T.B., Hua, J., Lehman, T.J., Harley, J.B., and Crow, M.K. 2007. High serum IFN-alpha activity is a heritable risk factor for systemic lupus erythematosus. *Genes Immun* 8:492-502.

6.   Niewold, T.B., Hua, J., Lehman, T.J., Harley, J.B., and Crow, M.K. 2007. High serum IFN-alpha activity is a heritable risk factor for systemic lupus erythematosus. *Genes Immun* 8:492-502.

7.   Weckerle, C.E., Franek, B.S., Kelly, J.A., Kumabe, M., Mikolaitis, R.A., Green, S.L., Utset, T.O., Jolly, M., James, J.A., Harley, J.B., et al. 2011. Network analysis of associations between serum interferon-alpha activity, autoantibodies, and clinical features in systemic lupus erythematosus. *Arthritis Rheum* 63:1044-1053.

8.   Niewold, T.B., Rivera, T.L., Buyon, J.P., and Crow, M.K. 2008. Serum type I interferon activity is dependent on maternal diagnosis in anti-SSA/Ro-positive mothers of children with neonatal lupus. *Arthritis Rheum* 58:541-546.

9.   Niewold, T.B., Kariuki, S.N., Morgan, G.A., Shrestha, S., and Pachman, L.M. 2009. Elevated serum interferon-alpha activity in juvenile dermatomyositis: associations with disease activity at diagnosis and after thirty-six months of therapy. *Arthritis Rheum* 60:1815-1824.

10.   Agik, S., Franek, B.S., Kumar, A.A., Kumabe, M., Utset, T.O., Mikolaitis, R.A., Jolly, M., and Niewold, T.B. 2012. The autoimmune disease risk allele of UBE2L3 in African American patients with systemic lupus erythematosus: a recessive effect upon subphenotypes. *The Journal of rheumatology* 39:73-78.

11.   Coxon, A., Rieu, P., Barkalow, F.J., Askari, S., Sharpe, A.H., von Andrian, U.H., Arnaout, M.A., and Mayadas, T.N. 1996. A novel role for the beta 2 integrin CD11b/CD18 in neutrophil apoptosis: a homeostatic mechanism in inflammation. *Immunity* 5:653-666.

12.   Thacker, S.G., Zhao, W., Smith, C.K., Luo, W., Wang, H., Vivekanandan-Giri, A., Rabquer, B.J., Koch, A.E., Pennathur, S., Davidson, A., et al. 2012. Type I interferons modulate vascular function, repair, thrombosis, and plaque

progression in murine models of lupus and atherosclerosis. *Arthritis Rheum* 64:2975-2985.

13.   Yuen, P.S., Dunn, S.R., Miyaji, T., Yasuda, H., Sharma, K., and Star, R.A. 2004. A simplified method for HPLC determination of creatinine in mouse serum. *Am J Physiol Renal Physiol* 286:F1116-1119.

14.   Figueiredo, N., Chora, A., Raquel, H., Pejanovic, N., Pereira, P., Hartleben, B., Neves-Costa, A., Moita, C., Pedroso, D., Pinto, A., et al. 2013. Anthracyclines induce DNA damage response-mediated protection against severe sepsis. *Immunity* 39:874-884.

15.   Rutigliano, J.A., Sharma, S., Morris, M.Y., Oguin, T.H., 3rd, McClaren, J.L., Doherty, P.C., and Thomas, P.G. 2014. Highly pathological influenza A virus infection is associated with augmented expression of PD-1 by functionally compromised virus-specific CD8+ T cells. *Journal of virology* 88:1636-1651.

16.   Han, C., Jin, J., Xu, S., Liu, H., Li, N., and Cao, X. 2010. Integrin CD11b negatively regulates TLR-triggered inflammatory responses by activating Syk and promoting degradation of MyD88 and TRIF via Cbl-b. *Nat Immunol* 11:734-742.

17.   Gabeler, E.E., van Hillegersberg, R., Statius van Eps, R.G., Sluiter, W., Gussenhoven, E.J., Mulder, P., and van Urk, H. 2002. A comparison of balloon injury models of endovascular lesions in rat arteries. *BMC Cardiovasc Disord* 2:16.

18.   Khan, S.J., Pham, S., Wei, Y., Mateo, D., St-Pierre, M., Fletcher, T.M., and Vazquez-Padron, R.I. 2010. Stress-induced senescence exaggerates postinjury

neointimal formation in the old vasculature. *Am J Physiol Heart Circ Physiol* 298:H66-74.

19.   Maiguel, D., Faridi, M.H., Wei, C., Kuwano, Y., Balla, K.M., Hernandez, D., Barth, C.J., Lugo, G., Donnelly, M., Nayer, A., et al. 2011. Small molecule-mediated activation of the integrin CD11b/CD18 reduces inflammatory disease. *Science signaling* 4:ra57.

20.   MacPherson, M., Lek, H.S., Prescott, A., and Fagerholm, S.C. 2011. A systemic lupus erythematosus-associated R77H substitution in the CD11b chain of the Mac-1 integrin compromises leukocyte adhesion and phagocytosis. *J Biol Chem* 286:17303-17310.

21.   Fuss, I.J., Kanof, M.E., Smith, P.D., and Zola, H. 2009. Isolation of whole mononuclear cells from peripheral blood and cord blood. *Curr Protoc Immunol* Chapter 7:Unit7 1.

22.   Lacey, D.C., Achuthan, A., Fleetwood, A.J., Dinh, H., Roiniotis, J., Scholz, G.M., Chang, M.W., Beckman, S.K., Cook, A.D., and Hamilton, J.A. 2012. Defining GM-CSF- and macrophage-CSF-dependent macrophage responses by in vitro models. *J Immunol* 188:5752-5765.

23.   Mia, S., Warnecke, A., Zhang, X.M., Malmstrom, V., and Harris, R.A. 2014. An optimized protocol for human M2 macrophages using M-CSF and IL-4/IL-10/TGF-beta yields a dominant immunosuppressive phenotype. *Scand J Immunol* 79:305-314.

24. Zhang, X., Goncalves, R., and Mosser, D.M. 2008. The isolation and characterization of murine macrophages. *Curr Protoc Immunol* Chapter 14:Unit 14 11.

25. Chevrier, N., Mertins, P., Artyomov, M.N., Shalek, A.K., Iannacone, M., Ciaccio, M.F., Gat-Viks, I., Tonti, E., DeGrace, M.M., Clauser, K.R., et al. 2011. Systematic discovery of TLR signaling components delineates viral-sensing circuits. *Cell* 147:853-867.

26. Ajroud, K., Sugimori, T., Goldmann, W.H., Fathallah, D.M., Xiong, J.P., and Arnaout, M.A. 2004. Binding Affinity of Metal Ions to the CD11b A-domain Is Regulated by Integrin Activation and Ligands. *J Biol Chem* 279:25483-25488.

27. Lee, J.O., Rieu, P., Arnaout, M.A., and Liddington, R. 1995. Crystal structure of the A domain from the alpha subunit of integrin CR3 (CD11b/CD18). *Cell* 80:631-638.

28. Xiong, J.P., Li, R., Essafi, M., Stehle, T., and Arnaout, M.A. 2000. An isoleucine-based allosteric switch controls affinity and shape shifting in integrin CD11b A-domain. *J Biol Chem* 275:38762-38767.

29. Berendsen, H.J.C., van der Spoel, D., and van Drunen, D. 1995. GROMACS: a message-passing parallel molecular dynamics implementation. *J. Comput. Phys. Commun.* 91:43-56.

30. Lindahl, E., Hess, B., and van der Spoel, D. 2001. GROMACS 3.0: a package for molecular simulation and trajectory analysis. *J. Mol. Model.* 7:306-317.

31. Kaminski, G.A., Friesner, R.A., Tirado-Rives, J., and Jorgensen, W.L. 2001. Evaluation and Reparametrization of the OPLS-AA Force Field for Proteins via

Comparison with Accurate Quantum Chemical Calculations on Peptides†. *J. Phys. Chem. B* 105:6474-6487.

32.   Miyamoto, S., and Kollman, P.A. 1992. Settle: An analytical version of the SHAKE and RATTLE algorithm for rigid water models. *J. Comput. Chem.* 13:952-962.

33.   Hess, B., Bekker, H., Berendsen, H.G.C., and Fraaije, J.G.E.M. 1997. LINCS: A linear constraint solver for molecular simulations. *J. Comput. Chem.* 18:1463-1472.

34.   Darden, T.A., York, D., and Pedersen, L. 1993. Particle mesh Ewald: An Nlog(N) method for Ewald sums in large systems. *J. Chem. Phys.* 98:10089-10092.

35.   Hockney, R.W., Goel, S.P., and Eastwood, J. 1974. Quiet high-resolution computer models of a plasma. *J. Comput. Phys.* 14:148-158.

36.   Krieger, E., and Vriend, G. 2002. Models@Home: distributed computing in bioinformatics using a screensaver based approach. *Bioinformatics* 18:315-318.

37.   Daura, X., van Gunsteren, W.F., and Mark, A.E. 1999. Folding-unfolding thermodynamics of a beta-heptapeptide from equilibrium simulations. *Proteins* 34:269-280.

38.   Trott, O., and Olson, A.J. 2010. AutoDock Vina: improving the speed and accuracy of docking with a new scoring function, efficient optimization, and multithreading. *J. Comput. Chem.* 31:455-461.

39.   Oostenbrink, C., Villa, A., Mark, A.E., and van Gunsteren, W.F. 2004. A biomolecular force field based on the free enthalpy of hydration and solvation: the

GROMOS force-field parameter sets 53A5 and 53A6. *J. Comput. Chem.* 25:1656-1676.

40.   Kabsch, W., and Sander, C. 1983. Dictionary of protein secondary structure: pattern recognition of hydrogen-bonded and geometrical features. *Biopolymers* 22:2577-2637.

41.   Chen, J., Salas, A., and Springer, T.A. 2003. Bistable regulation of integrin adhesiveness by a bipolar metal ion cluster. *Nat Struct Biol* 10:995-1001.

42.   Gupta, V., Gylling, A., Alonso, J.L., Sugimori, T., Ianakiev, P., Xiong, J.P., and Arnaout, M.A. 2007. The beta-tail domain (betaTD) regulates physiologic ligand binding to integrin CD11b/CD18. *Blood* 109:3513-3520.

43.   Lee, J.C., Espeli, M., Anderson, C.A., Linterman, M.A., Pocock, J.M., Williams, N.J., Roberts, R., Viatte, S., Fu, B., Peshu, N., et al. 2013. Human SNP links differential outcomes in inflammatory and infectious disease to a FOXO3-regulated pathway. *Cell* 155:57-69.

44.   Faridi, M.H., Altintas, M.M., Gomez, C., Duque, J.C., Vazquez-Padron, R.I., and Gupta, V. 2013. Small molecule agonists of integrin CD11b/CD18 do not induce global conformational changes and are significantly better than activating antibodies in reducing vascular injury. *Biochim Biophys Acta* 1830:3696-3710.

45.   Jin, M., Andricioaei, I., and Springer, T.A. 2004. Conversion between three conformational states of integrin I domains with a C-terminal pull spring studied with molecular dynamics. *Structure* 12:2137-2147.

46. Salas, A., Shimaoka, M., Phan, U., Kim, M., and Springer, T.A. 2006. Transition from rolling to firm adhesion can be mimicked by extension of integrin alphaLbeta2 in an intermediate affinity state. *J Biol Chem* 281:10876-10882.

47. Mc, G.H., Jr., Geer, J.C., and Holman, R.L. 1957. Sites of vascular vulnerability in dogs demonstrated by Evans blue. *AMA Arch Pathol* 64:303-311.

48. Jaffe, E.A., Hoyer, L.W., and Nachman, R.L. 1973. Synthesis of antihemophilic factor antigen by cultured human endothelial cells. *J Clin Invest* 52:2757-2764.

49. Chen, D., Asahara, T., Krasinski, K., Witzenbichler, B., Yang, J., Magner, M., Kearney, M., Frazier, W.A., Isner, J.M., and Andres, V. 1999. Antibody blockade of thrombospondin accelerates reendothelialization and reduces neointima formation in balloon-injured rat carotid artery. *Circulation* 100:849-854.

50. Semmrich, M., Smith, A., Feterowski, C., Beer, S., Engelhardt, B., Busch, D.H., Bartsch, B., Laschinger, M., Hogg, N., Pfeffer, K., et al. 2005. Importance of integrin LFA-1 deactivation for the generation of immune responses. *J Exp Med* 201:1987-1998.

51. Park, E.J., Peixoto, A., Imai, Y., Goodarzi, A., Cheng, G., Carman, C.V., von Andrian, U.H., and Shimaoka, M. 2010. Distinct roles for LFA-1 affinity regulation during T-cell adhesion, diapedesis, and interstitial migration in lymph nodes. *Blood* 115:1572-1581.

52. Park, E.J., Mora, J.R., Carman, C.V., Chen, J., Sasaki, Y., Cheng, G., von Andrian, U.H., and Shimaoka, M. 2007. Aberrant activation of integrin alpha4beta7 suppresses lymphocyte migration to the gut. *J Clin Invest* 117:2526-2538.

53.   Xie, C., Zhu, J., Chen, X., Mi, L., Nishida, N., and Springer, T.A. 2010. Structure

of an integrin with an alphaI domain, complement receptor type 4. *EMBO J*

29:666-679.

Supplemental Figures and Figure Legends
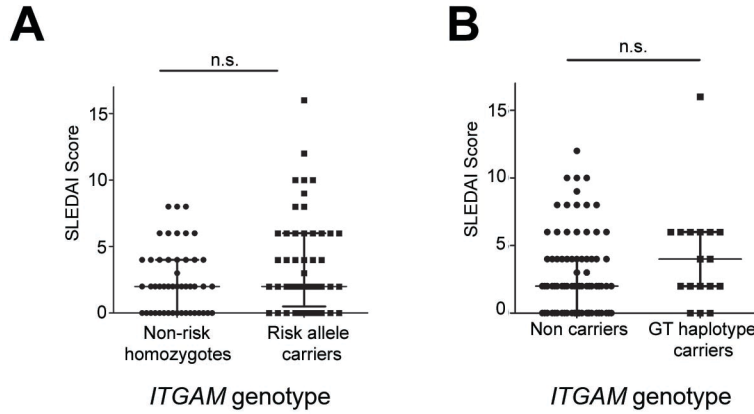
Figure S1. SLE Disease Activity Index (SLEDAI) scores in SLE patients at the time of blood sampling, stratified by *ITGAM* genotype. Patients are separated using the same groups in panels A. and B. as was done in Figure 1A and 1B respectively. SLEDAI scores are compared between genotype groups using the Mann-Whitney U test, with no significant differences observed (n.s.). Central tendency is represented by the median, and error bars show the interquartile range.

A

CD11b

R77H

N- 1 2 | αA-domain | 3 4 5 6 7 | Thigh | Calf-1* | Calf-2 | TM | Cytopl. Tail*

β-propeller ∟insert∟ β-propeller domain

A858V*   P1146S*

CD18

N- PSI | βA-domain | 1 2 3 4 | βTD | TM | Cytoplasmic Tail

Hybrid domain ∟insert∟ Hybrid domain

B

R77H

A858V

CD11bA (αA-domain)

P1146S

C

LA1

MIDAS

F

α7

LA1

D

E

RMSD of LA1-removed structure after 30ns.

— Closed
— Open
— LA1 docked and minimized (intermediate)
— LA1-docked structure, after LA1 removal and 30ns MD

α1 helix   F-α7 Loop   α7 helix

F

RMSD of various regions of CD11b in the energy-minimized, LA1 removed structure from the CD11bA closed conformation	RMSD (Å)
F-α7 loop	1.4092
α7 helix	3.4962
CD11bA domain	2.6593

G

F-α7 loop

MD →

α7   α7   F   α7

Figure S2. Molecular dynamics simulations show that LA1 induces partially active, intermediate affinity conformation in the CD11bA. A. A diagram showing domain organization of the CD11b and the CD18 chains. Sites of mutations encoded by the three ITGAM SNPs under study here are also depicted. **B.** A ribbon model of integrin CD11b/CD18 in its bent conformation based on the published structure of αXβ2 (53). The model also depicts the proposed locations of the three mutations encoded by the three ITGAM SNPs under study here. **C.** Chemical structure of LA1. Also shown is a computational model of the LA1 bound CD11bA, displaying LA1 (red stick model) docked present in the activation-sensitive allosteric pocket near the F-α7 region of CD11bA (white ribbon). A metal ion at the MIDAS site is shown as a blue sphere. **D**. Graph showing computed root-mean-square-deviation (RMSD) of the CD11bA domain after removal of LA1 from the LA1-docked structure. Molecular dynamics simulation of LA1-docked CD11bA structure was performed for 30ns, after removal of LA1 from the binding pocket, and it showed conformational changes in the LA1-removed CD11bA that stabilized after 8ns of simulation, into a conformation that resembled the closed form. These molecular dynamics studies suggest that LA1 induces intermediate affinity conformation in the CD11bA, thereby priming the integrin for ligand binding. **E**. Graph showing computed RMSD values of different regions of the CD11bA domain (amino acid residue numbers on x-axis), after molecular dynamics simulation of various forms. It shows a large movement in the F-α7 loop, α7 helix and the α1 helix regions between the LA1-docked and LA1-removed structures that stabilized after 8ns of simulation, into a conformation that resembled the closed form. **F**. Table showing calculated RMSD values between LA1-docked and LA1-removed forms of CD11bA for various regions of

CD11bA. **G.** A superposition of the most representative structures of different forms of the CD11bA domain derived from MD simulations. The superimposed ribbon diagrams show structures of x-ray derived CD11b in the closed conformation (yellow ribbon) (27) and open conformation (28) (blue ribbon) were superimposed with an energy minimized structure of LA1-bound CD11bA (19) (LA1 is omitted for clarity) prior to molecular dynamics (MD) simulation (left figure, CD11bA is shown as red ribbon) and after a 30ns MD simulation (right figure, CD11bA is shown as pink ribbon). A zoomed-in view of the activation-sensitive F-α7 region is presented in the inset, where all four structures have been superimposed to show the conformational changes upon MD simulation.
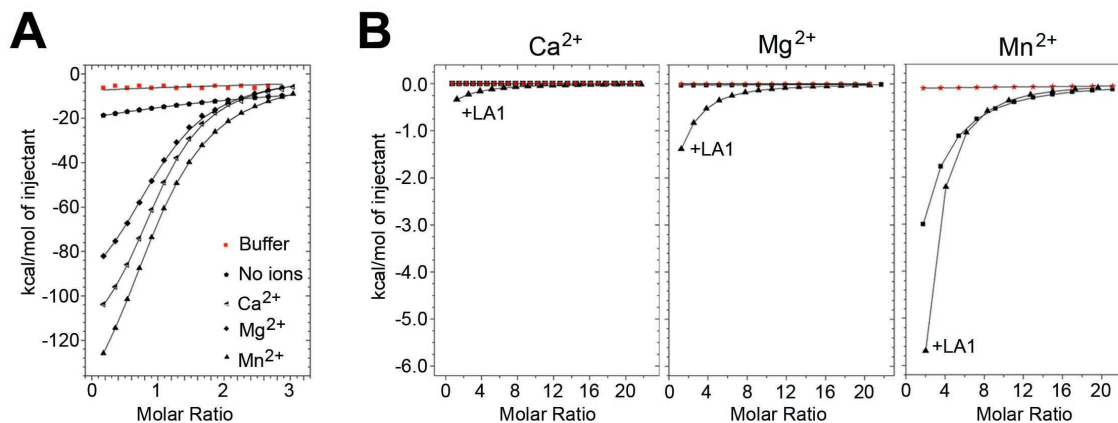
Figure S3. Isothermal titration calorimetry (ITC) based measurement of LA1 binding to CD11bA. A. Results of isothermal titration calorimetry (ITC) based measurements of LA1 binding to CD11bA in the absence or presence of various divalent ions at 298K (25°C). The graph shows integrated heats of reaction derived from the binding of LA1, in the reaction cell, when titrated with CD11bA in the presence of various metal ions, as shown. The solid lines represent the least square fit to a single binding model. **D.** The graphs show integrated heats of reaction derived from the binding of CD11bA in the reaction cell, in the absence or presence of three different metal ions, as indicated, when titrated with a solution of LA1. The solid lines represent the least square fit to a single binding model.
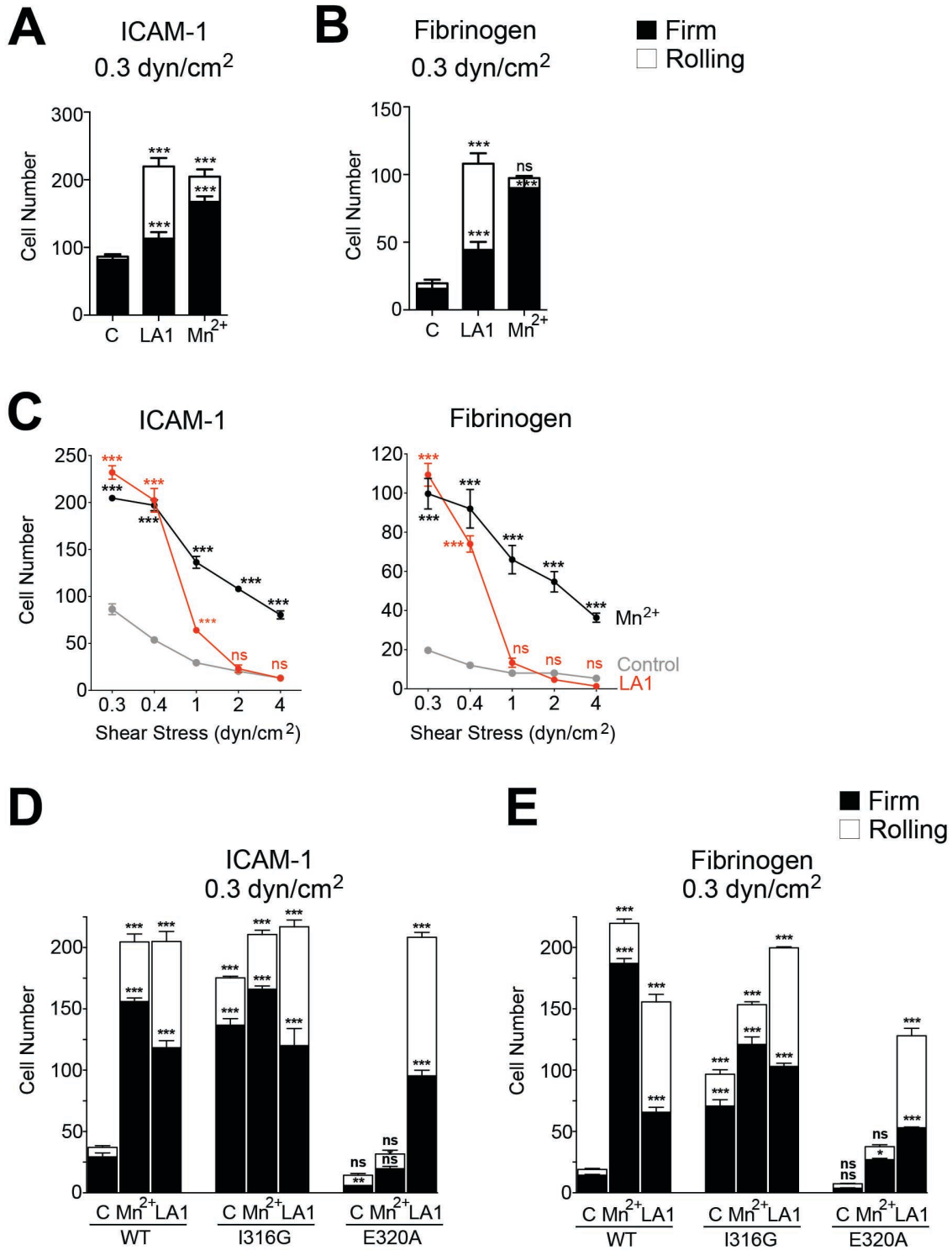
Figure S4. LA1 binding enhances rolling adhesion of CD11b-expressing cells under shear stress. A-B. Adhesive behavior of vehicle (C), Mn^{2+}, or LA1-treated

CD11b/CD18-expressing cells to immobilized ligand ICAM-1 (**A**) or to fibrinogen (**B**) under the wall shear stress of 0.3 dyn/cm^2. Bars show mean $\pm$ SD (n=3) from one of at least three independent experiments. (***P <0.001, ns = not significant, Student's t-test). **C.** Cell resistance to detachment in shear flow. Graphs show total number of CD11b/CD18-expressing cells remaining bound at the end of each shear stress. Each data point shows the number of cells remaining bound (mean $\pm$ SD) (n=3) from one of at least three independent experiments. (***P <0.001, ns = not significant, Student's t-test). **D.** Graph showing adhesion of cells expressing CD11bWT/CD18, CD11bI316G/CD18 or CD11bE320A/CD18 to immobilized ligand ICAM-1 in DMSO (C), Mn^{2+} or LA1 under a constant wall shear stress of 0.3 dyn/cm^2. Bars show mean $\pm$ the standard deviation (SD) (n=3) of cumulative number of firmly adherent and rolling cells. Data is from one of at least three independent experiments. (***P <0.001, ns = not significant, Student's t-test). **E.** Graph showing adhesion of cells expressing CD11bWT/CD18, CD11bI316G/CD18 or CD11bE320A/CD18 to immobilized ligand Fibrinogen in DMSO (C), Mn^{2+} or LA1 under a constant wall shear stress of 0.3 dyn/cm^2. Bars show mean $\pm$ the standard deviation (SD) (n=3) and are from one of at least three independent experiments. (***P <0.001, ns = not significant, Student's t-test).
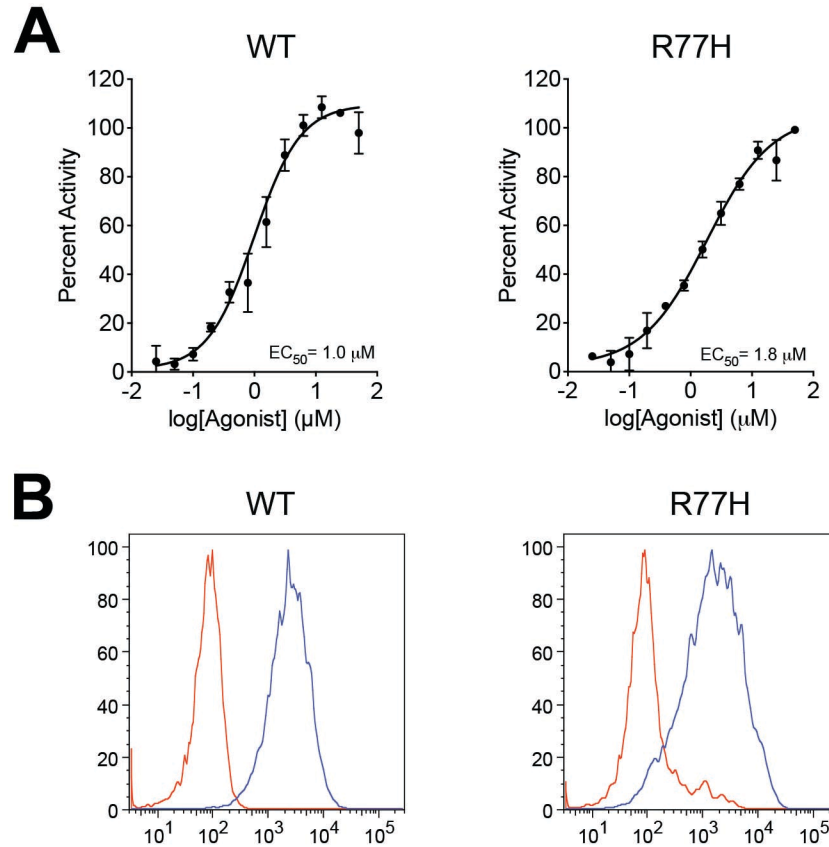
Figure S5. LA1 increases adhesion of WT and R77H mutant integrin CD11b/CD18 to similar levels. A. Dose-response curves showing the percentages of input K562 CD11b/CD18 WT (**A**) or R77H (**B**) CD11b/CD18 cells (with similar expression levels, see **B** below) adhering to immobilized fibrinogen in the presence of increasing concentration of LA1. EC50 values are indicated on each graph. Data shown are means $\pm$ SEM (n = 3 replicates per data point) and are from one of at least three independent experiments. **B.** Flow cytometric analysis showing similar level of CD11b/CD18 surface expression on live K562 cells stably transfected with CD18 and CD11b WT or CD11b R77H and analyzed using the anti-CD11b/CD18 mAb IB4 (blue trace) or an IgG2a isotype control (red trace). Data shown are representative of at least two independent experiments.
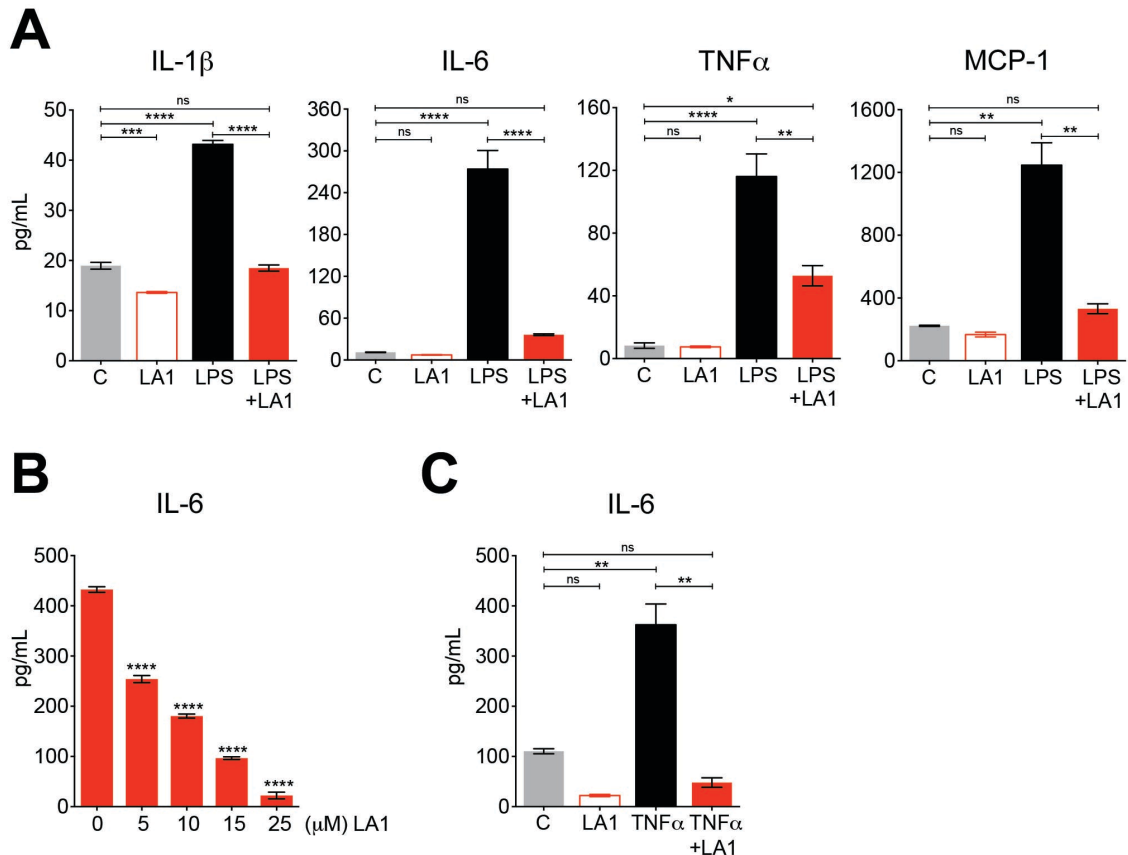
Figure S6. LA1 treatment suppresses synthesis of pro-inflammatory chemokines and cytokines in TLR4-stimulated primary neutrophils and macrophages. A. ELISA-based quantification of IL-1β, IL6, TNF and MCP-1 levels in supernatants of mouse neutrophils treated with vehicle DMSO (C), LA1 (15 μM), LPS (100ng/mL) or LPS (100ng/mL) and LA1 (15 μM) for 8 hrs (IL-1β, IL6 and MCP-1) or 12 hrs (TNF). Bars show mean ± the standard error of the mean (SEM) (n=3) from one of at least two independent experiments. (*P <0.05, **P <0.01, ****P <0.0001, ns = not significant, One-way ANOVA, Tukey's test). **B.** Bar graph showing ELISA based quantification of IL6 levels in supernatants of C57BL/6 WT bone marrow derived macrophages stimulated with LPS (100ng/mL) in the presence of various concentrations of LA1 for 12 hrs. Bars show mean ± SEM (n=3) from one of at least two independent experiments. (****P

<0.0001, ns = not significant, Student's t-test). **C.** Bar graph (mean $\pm$ SEM) showing ELISA based quantification of IL6 levels in supernatants of C57BL/6 WT mouse neutrophils treated with vehicle DMSO (C), LA1 (15 µM), TNFα (20ng/mL) or TNFα (20ng/mL) and LA1 (15 µM) for 12 hrs. Data are from one of at least two independent experiments. (**P <0.01, ns = not significant, One-way ANOVA, Tukey's test).
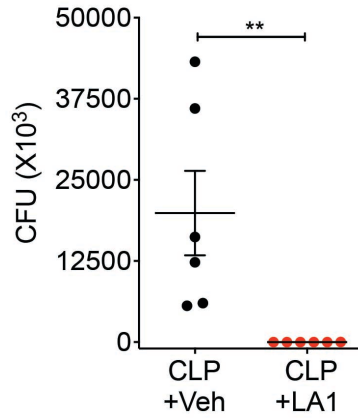
Figure S7. CFU count in CLP mice. Graph showing polymicrobial load (CFUs) in blood of B6 WT animals undergoing CLP and treated with vehicle or LA1 24 hr post-CLP. Each circle represents data from individual animal. Horizontal lines indicate arithmetic mean ± SEM. (**P <0.01, Student's t-test).

A

#	Enriched Canonical Pathways	Total Genes	In Dataset	-log (p-value)	FDR
1	Immune response_Antiviral actions of Interferons	52	13	11.87	5.4E-10
2	Immune response_IFN alpha/beta signaling pathway	24	8	8.59	5.1E-07
3	Immune response_Th1 and Th2 cell differentiation	40	8	6.67	2.8E-05
4	PDE4 regulation of cyto/chemokine expression in inflammatory skin diseases	50	8	5.89	1.3E-04
5	Immune response_Differentiation and clonal expansion of CD8+ T cells	39	7	5.56	2.2E-04
6	Immune response_Role of PKR in stress-induced antiviral cell response	57	8	5.44	2.2E-04
7	Immune response_Role of HMGB1 in dendritic cell maturation and migration	27	6	5.41	2.2E-04
8	Immune response_Oncostatin M signaling via JAK-Stat in mouse cells	18	5	5.10	4.0E-04
9	Immune response_CD40 signaling	65	8	5.00	4.4E-04
10	Immune response_Oncostatin M signaling via JAK-Stat in human cells	20	5	4.85	5.6E-04

B

#	Enriched Cellular and Molecular Processes	Total Genes	In Dataset	-log (p-value)	FDR
1	Inflammation_Interferon signaling	110	32	25.45	4.7E-24
2	Immune response_Innate immune response to RNA viral infection	85	17	10.69	1.3E-09
3	Inflammation_Jak-STAT Pathway	186	20	7.51	1.4E-06
4	Proliferation_Negative regulation of cell proliferation	184	18	6.18	2.0E-05
5	Cell adhesion_Leucocyte chemotaxis	205	19	6.13	2.0E-05
6	Chemotaxis	137	15	5.84	3.1E-05
7	Inflammation_IL-12,15,18 signaling	59	10	5.78	3.1E-05
8	Inflammation_IFN-gamma signaling	110	13	5.50	5.2E-05
9	Proliferation_Lymphocyte proliferation	209	18	5.37	6.2E-05
10	Immune response_Th17-derived cytokines	98	12	5.28	6.9E-05

C

#	Enriched Diseases	Total Genes	In Dataset	-log (p-value)	FDR
1	Autoimmune Diseases	2868	155	48.67	3.1E-46
2	Connective Tissue Diseases	2177	134	47.17	4.9E-45
3	Lupus Erythematosus, Systemic	1221	98	42.83	7.2E-41
4	Infection	1185	96	42.22	2.2E-40
5	Bacterial Infections and Mycoses	1307	100	41.93	3.4E-40
6	Virus Diseases	1531	96	32.92	2.9E-31
7	Immune System Diseases	6296	200	30.40	8.2E-29
8	RNA Virus Infections	1055	77	30.26	1.0E-28
9	Joint Diseases	1713	95	28.36	7.0E-27
10	Arthritis	1683	94	28.27	7.8E-27

D

#	Enriched GO Processes	Total Genes	In Dataset	-log (p-value)	FDR
1	immune response	1654	135	61.76	8.4E-59
2	defense response	1915	135	54.00	2.4E-51
3	immune system process	2833	160	52.72	3.1E-50
4	response to biotic stimulus	1220	107	50.40	4.8E-48
5	response to other organism	1172	104	49.32	4.2E-47
6	response to external biotic stimulus	1173	104	49.29	4.2E-47
7	response to virus	382	62	43.92	8.5E-42
8	defense response to virus	212	48	41.02	5.8E-39
9	innate immune response	1093	89	38.59	1.4E-36
10	response to stress	4374	176	38.09	3.9E-36

Figure S8. Antiviral immune response canonical pathways are enriched in LPS-stimulated human macrophages treated with LA1. A. Graph (left) of a table (middle) showing the top 10 significant canonical pathways that are enriched in the 416 genes that were significantly changed in macrophages treated with LPS+LA1 vs LPS, upon analysis of microarray data using GeneGo. The bar graph (left) shows P-value associated with enrichment. A graphical representation of the enriched pathway from GeneGo is

presented on the right. The blue hexagon denotes the ratio of number of genes present in our dataset over the total number of genes in that particular pathway. **B.** A table showing the top 10 significant Cellular and Molecular Processes that are enriched in the 416 genes that were significantly changed in macrophages treated with LPS+LA1 vs LPS, upon analysis of microarray data using GeneGo. **C.** A table showing the top 10 significantly enriched disease categories in the 416 genes that were significantly changed in macrophages treated with LPS+LA1 vs LPS, upon analysis of microarray data using GeneGo. Autoimmune diseases and SLE are among the top. **D.** A table showing the top 10 significantly enriched GO categories in the 416 genes that were significantly changed in macrophages treated with LPS+LA1 vs LPS, upon analysis of microarray data using GeneGo. Immune response is at the top.
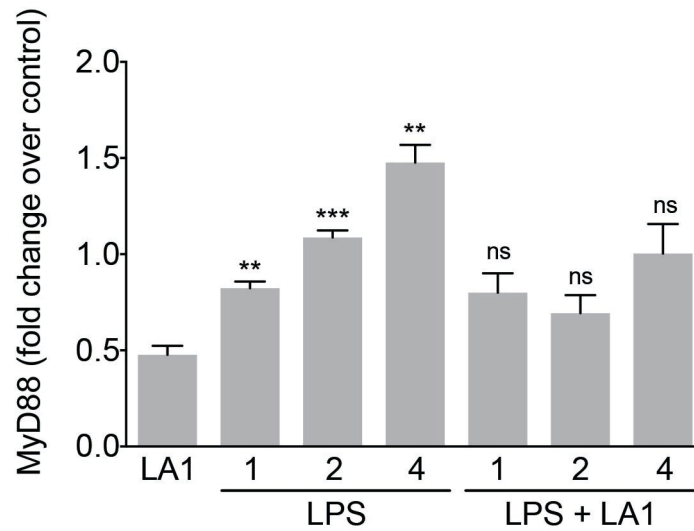
Figure S9. LA1-mediated CD11b activation reduces LPS-stimulated expression of MyD88. Bar graph (mean $\pm$ SEM (n=3)) showing densitometric quantification of MyD88 levels in the immunoblots from lysates of RAW macrophages stimulated with LPS for 0-4h in the absence or presence of LA1, as presented in Figure 3D in the main text, showing that LA1-mediated CD11b activation significantly reduced MyD88 levels. Expression was normalized relative to GAPDH levels. (**P <0.01, ***P <0.001, ns = not significant, Student's t-test).
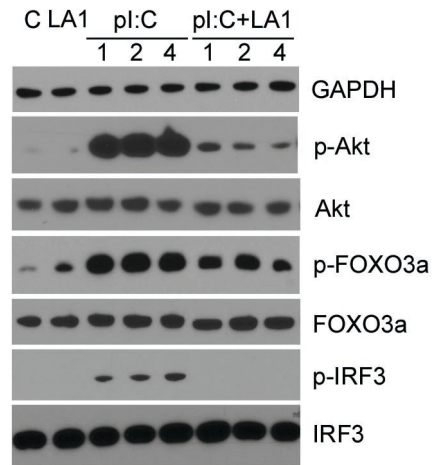
Figure S10. LA1-mediated CD11b activation suppresses TLR3-dependent IFN signaling via Akt-FOXO3-IRF3 axis. Immunoblot analysis of various phosphorylated (p-) and total proteins in lysates of RAW macrophages stimulated with pI:C for 0-4h in the absence or presence of LA1. GAPDH was used as loading control.
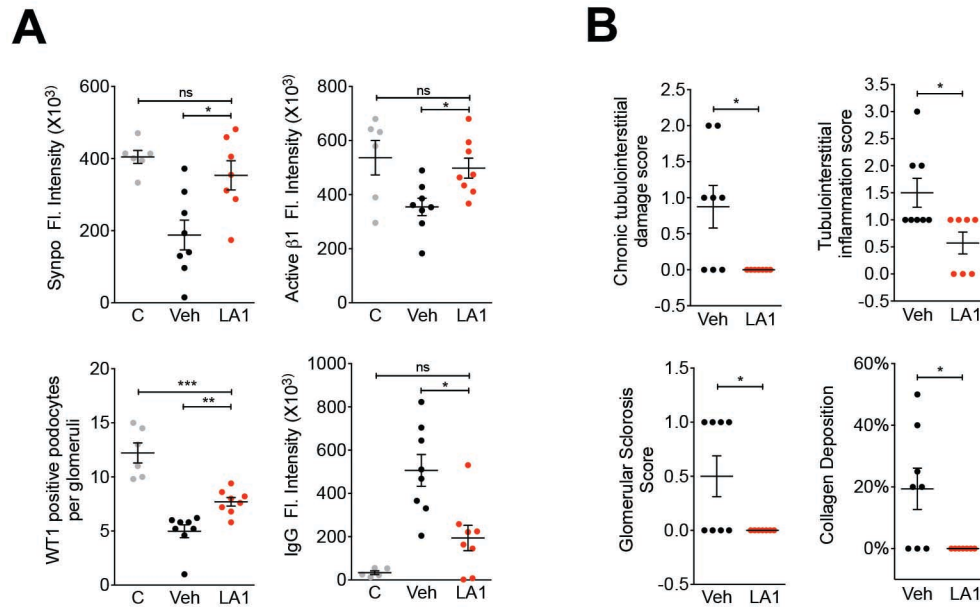
Figure S11. LA1-treated lupus-prone mice show reduced glomerular damage. A. Graphs showing quantification of immunostaining in fluorescently-labeled kidney sections from 19-week old control (MRL/*Mpj*) and lupus-prone MRL/*lpr* mice, treated with either vehicle or LA1 (as shown in Fig. 4E). Kidney sections stained with antibodies against the podocyte markers synaptopodin, WT1, active integrin β1 or anti-IgG (to quantify immune complex deposition) were quantified. Individual data points are displayed and line represents mean ± SEM (n=5 for MRL/*Mpj*, n=7 LA1-treated MRL/*lpr* mice and n=8 vehicle-treated Mrl/*lpr* mice); C is MRL/*Mpj*, veh is vehicle treated MRL/lpr, **B.** Kidney damage scores from kidney tissue from MRL/*lpr* vehicle versus LA1 treated mice, as assessed by histochemical analyses for tubulointerstitial damage, glomerulosclerosis and collagen deposition. Individual data points are shown. Line indicates mean ± SEM (n=7 LA1-treated MRL/*lpr* mice and n=8 vehicle-treated MRL/*lpr* mice). (*P <0.05, **P <0.01, ***P <0.001, ****P <0.0001, ns = not significant, Student's t-test).
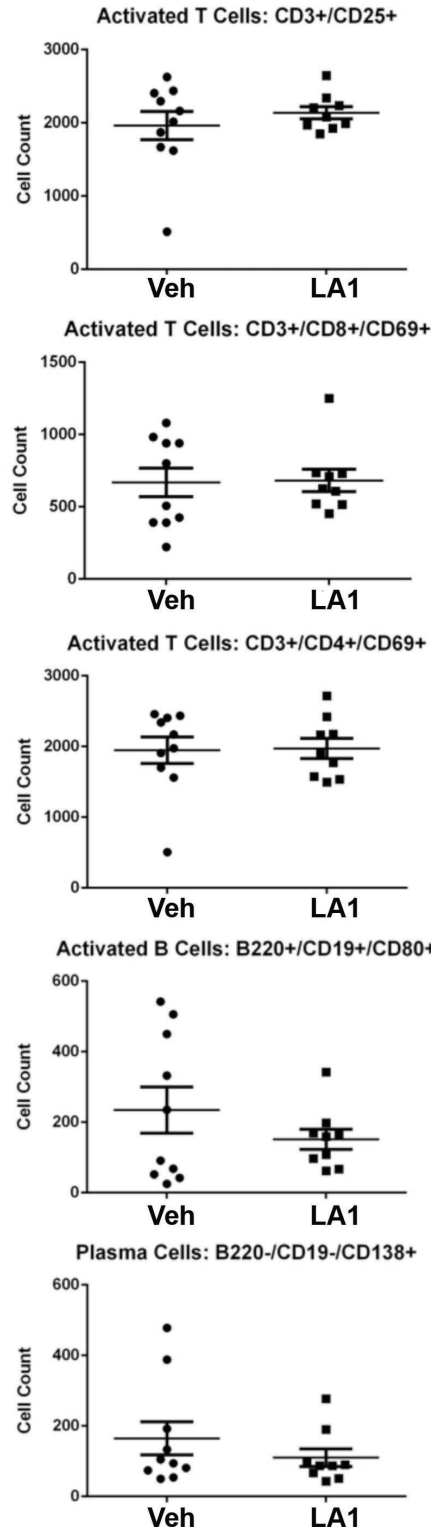
Figure S12. Effect of LA1 on splenic cell subsets. Graphs represent splenic cell counts

for specific cell subsets in individual mice from LA1-treated and vehicle-treated MRL/lpr

mice, at euthanasia, at 19 weeks of age (n=10 in vehicle-treated and n=9 in LA1-treated). Y-axis represents cell counts of specific cell subset/1×10^6 splenocytes. Horizontal lines are mean+SEM and the dots represent values in individual mice. All comparisons are non-significant.
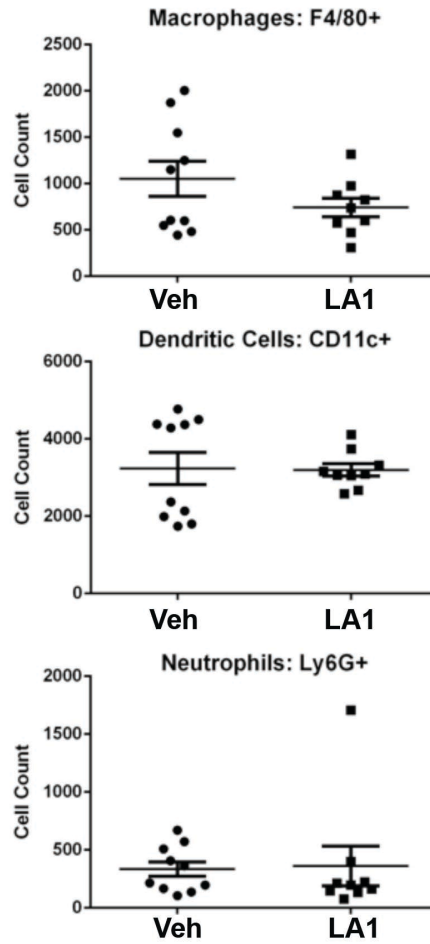
Figure S13. Effect of LA1 on splenic myeloid cell subsets. Graphs represent splenic cell counts for specific cell subsets in individual mice from LA1-treated and vehicle-treated MRL/lpr mice, at euthanasia, at 19 weeks of age (n=10 in vehicle-treated and n=9 in LA1-treated). Y-axis represents cell counts of specific cell subset/1×10^{6} splenocytes. Horizontal lines are mean+SEM and the dots represent values in individual mice. All comparisons are non-significant.
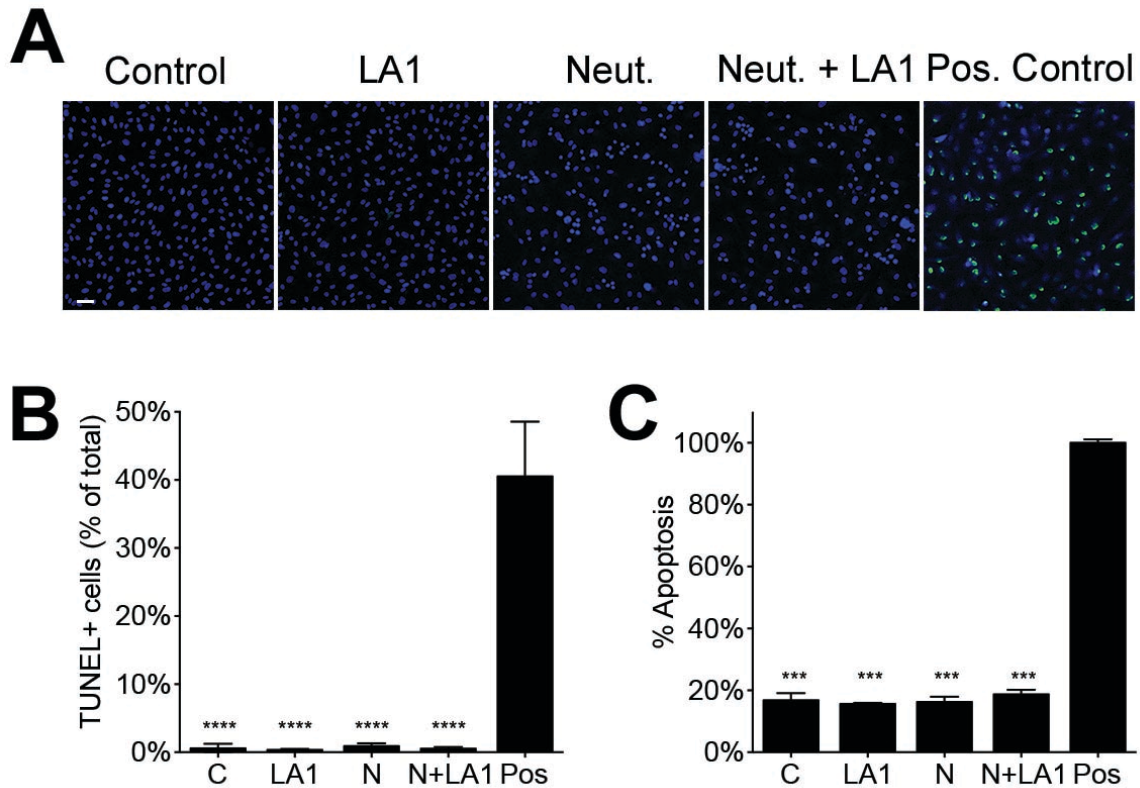
Figure S14. LA1 does not damage endothelial cells. A. Representative confocal images of human umbilical vein endothelial cells (HUVECs) cultured in the absence or presence of LA1 and neutrophils (DAPI-stained nuclei (blue), TUNEL staining (green)). H_2O_2-treated HUVECS serve as positive control. Scale bar=50 μm. **B.** Quantification of TUNEL-positive cells as a percentage of total HUVECs from (A). Data shown are mean ± SEM from at least 5 independent fields, from duplicate experiments. **C.** Quantification of HUVEC apoptosis under various conditions (as in A) using LDH release assay and expressed as a percentage of total LDH in a positive control (cells lysed with 2% Triton-100). Data shown are mean ± SEM (n=3). (****P* <0.001, *****P* <0.0001, ns = not significant, Student's t-test).

Supplemental Tables

Table S1: Clinical and serologic characteristics of the SLE patients

	Clinical Feature	SLE Cases n=171
Demographic characteristics	Age, years*	50 (37-63)
	Female, no (%)	148 (87)
ACR Clinical Criteria for SLE	Malar rash, no (%)	89 (52)
	Discoid rash, no (%)	55 (32)
	Photosensitivity, no (%)	96 (56)
	Oral ulcers, no (%)	57 (33)
	Arthritis, no (%)	144 (84)
	Serositis, no (%)	57 (33)
	Renal disorder, no (%)	61 (36)
	Neurological disorder, no (%)	19 (11)
	Hematological disorder, no (%)	64 (30)
	Immunological disorder, no (%)	118 (69)
Prevalence of Specific Autoantibody Profiles	ANA, no (%)	160 (94)
	Ro, no (%)	63 (37)
	La, no (%)	30 (18)
	Sm, no (%)	34 (20)
	RNP, no (%)	47 (27)
	DNA, no (%)	94 (55)

* the age values are the median (interquartile range), other values represent the number of patients who have that categorical finding, followed by the percentage in parentheses.

Metal ion	CD11bA alone				CD11bA + LA1			
	K_d (µM)	ΔS^0 (kcal/mol/deg)	ΔH^0 (kcal/mol)	ΔG^0 (kcal/mol)	K_d (µM)	ΔS^0 (kcal/mol/deg)	ΔH^0 (kcal/mol)	ΔG^0 (kcal/mol)
Ca^{2+}	2041 ±500	3.629 ±0.02	-0.069 ±0.02	-3.698	43.8±12	0.34±0.01	-5.64±1.14	-5.980
Mg^{2+}	1096 ±306	3.349 ±0.01	-0.720 ±0.2	-4.069	27.5±8	0.02±0.001	-6.289±1.98	-6.269
Mn^{2+}	41.7 ±5	0.18 ±0.22	-6.19 ±1.20	-6.010	12.58±2	1.47±0.21	-8.29±1.30	-6.820

Table S2. Binding energy of CD11bA in the absence or presence of pre-bound LA1 to various metal ions.

CD11bA with metal ions	LA1 Binding			
	K_d (µM)	ΔS^0 (kcal/mol/deg)	ΔH^0 (kcal/mol)	ΔG^0 (kcal/mol)
None	47±9	-0.402±0.071	-127.1±1.07	-7.304
Ca^{2+}	0.9±0.02	-0.283±0.043	-92.69±0.12	-8.356
Mg^{2+}	1±0.07	-0.311±0.064	-100.9±1.01	-8.222
Mn^{2+}	1.6±0.2	-0.541±0.093	-169.3±1.56	-8.082

Table S3. Binding energy of LA1 to CD11bA in the absence or presence of various metal ions.

Table S4. mRNA expression of 416 genes is affected by LA1.

Table S4. mRNA expression of 416 genes is affected by LA1

	ProbeID	Accession	Entrez Gene_ID	Probe_Id	Symbol	[LPS](normalized)	[LPS + LA1](normalized)	p (Corr)	Fold Change	FC (abs)	Regulation	Significant
1	5570711	NM_002164.4	3620	ILMN_32399	IDO1	5.52	0.30	0.00	-37.03	37.03	down	yes
2	5570278	NM_002416.1	4283	ILMN_17453	CXCL9	4.75	-0.05	0.00	-27.76	27.76	down	yes
3	380259	NM_002164.3	3620	ILMN_16563	INDO	5.05	0.25	0.00	-27.72	27.72	down	yes
4	6270553	NM_001565.2	3627	ILMN_17917	CXCL10	5.73	0.98	0.00	-26.86	26.86	down	yes
5	870202	NM_003810.2	8743	ILMN_18013	TNFSF10	4.42	0.02	0.00	-21.14	21.14	down	yes
6	6620121	NM_005623.2	6355	ILMN_17729	CCL8	4.49	0.36	0.00	-17.56	17.56	down	yes
7	1980524	NM_052941.3	115361	ILMN_17713	GBP4	4.24	0.29	0.00	-15.43	15.43	down	yes
8	1030204	NM_002981.1	6346	ILMN_20869	CCL1	3.92	-0.01	0.00	-15.26	15.26	down	yes
9	3360343	NM_080657.4	91543	ILMN_16578	RSAD2	4.03	0.28	0.00	-13.46	13.46	down	yes
10	6520523	NM_145659.3	246778	ILMN_17537	IL27	3.56	0.00	0.00	-11.79	11.79	down	yes
11	1510364	NM_052942.2	115362	ILMN_21145	GBP5	3.98	0.48	0.00	-11.30	11.30	down	yes
12	4900435	NM_006573.3	10673	ILMN_17584	TNFSF13B	2.82	-0.64	0.00	-11.01	11.01	down	yes
13	3370349	NM_001710.4	629	ILMN_17742	CFB	3.74	0.37	0.00	-10.29	10.29	down	yes
14	1980750	NM_145641.1	80833	ILMN_17568	APOL3	3.03	-0.31	0.00	-10.12	10.12	down	yes
15	6330132	NM_002201.4	3669	ILMN_16599	ISG20	4.28	0.95	0.00	-10.00	10.00	down	yes
16	7320546	NM_014398.2	27074	ILMN_21708	LAMP3	3.37	0.21	0.00	-8.94	8.94	down	yes
17	6840020	NM_006573.3	10673	ILMN_20668	TNFSF13B	2.53	-0.57	0.00	-8.56	8.56	down	yes
18	7100646	NM_006274.2	6363	ILMN_17691	CCL19	3.22	0.12	0.00	-8.55	8.55	down	yes
19	4540709	NM_005409.3	6373	ILMN_20678	CXCL11	3.10	0.01	0.00	-8.51	8.51	down	yes
20	3180039	NM_015149.3	23179	ILMN_16543	RGL1	1.79	-1.27	0.00	-8.38	8.38	down	yes
21	1030333	NM_002982.3	6347	ILMN_17200	CCL2	1.82	-1.25	0.00	-8.37	8.37	down	yes
22	2190148	NM_002053.1	2633	ILMN_21487	GBP1	3.78	0.74	0.00	-8.24	8.24	down	yes
23	2810767	NM_005755.2	10148	ILMN_18026	EBI3	3.00	0.03	0.00	-7.86	7.86	down	yes
24	6840035	NM_002053.1	2633	ILMN_17011	GBP1	3.72	0.75	0.00	-7.83	7.83	down	yes
25	3710243	NM_024625.3	56829	ILMN_17299	ZC3HAV1	3.39	0.42	0.00	-7.80	7.80	down	yes
26	3870338	NM_006820.1	10964	ILMN_17239	IFI44L	2.91	-0.02	0.00	-7.63	7.63	down	yes
27	7400743	NM_020954.2	57714	ILMN_22890	KIAA1618	2.94	0.04	0.00	-7.47	7.47	down	yes
28	2000148	NM_001548.3	3434	ILMN_17076	IFIT1	4.06	1.22	0.00	-7.14	7.14	down	yes
29	5700725	NM_033255.2	94240	ILMN_23885	EPSTI1	2.91	0.08	0.00	-7.12	7.12	down	yes
30	5360156	NM_003641.3	8519	ILMN_18012	IFITM1	2.81	0.04	0.00	-6.83	6.83	down	yes
31	1690066	NM_002462.2	4599	ILMN_16623	MX1	3.33	0.64	0.00	-6.44	6.44	down	yes
32	7650097	NM_198213.1	8638	ILMN_16748	OASL	4.12	1.47	0.00	-6.27	6.27	down	yes
33	5490470	NM_002463.1	4600	ILMN_22319	MX2	2.94	0.30	0.00	-6.21	6.21	down	yes
34	6280543	NM_003733.2	8638	ILMN_16817	OASL	2.99	0.38	0.00	-6.09	6.09	down	yes
35	580678	NM_001080535.1	93082	ILMN_22358	LINCR	3.03	0.42	0.00	-6.08	6.08	down	yes
36	4040181	NM_001042483.1	26471	ILMN_24046	NUPR1	2.39	-0.22	0.00	-6.08	6.08	down	yes
37	1770593	NM_003956.3	9023	ILMN_17410	CH25H	2.56	-0.03	0.00	-6.00	6.00	down	yes
38	520408	NM_001549.2	3437	ILMN_22397	IFIT3	3.62	1.04	0.00	-5.97	5.97	down	yes
39	540670	NM_172374.1	259307	ILMN_16599	IL4I1	2.04	-0.51	0.00	-5.88	5.88	down	yes
40	2760500	NM_001775.2	952	ILMN_22337	CD38	2.56	0.03	0.00	-5.79	5.79	down	yes
41	5550035	NM_178452.3	123872	ILMN_17769	LRRC50	2.57	0.08	0.00	-5.63	5.63	down	yes
42	4760703	NM_014314.3	23586	ILMN_17970	DDX58	2.81	0.33	0.00	-5.58	5.58	down	yes
43	3940520	NM_001002010.1	51251	ILMN_23521	NT5C3	2.52	0.09	0.00	-5.41	5.41	down	yes
44	240053	NM_001024071.1	2643	ILMN_18127	GCH1	2.84	0.42	0.00	-5.36	5.36	down	yes
45	1770072	XM_001133269.2	730249	ILMN_31932	IRG1	3.38	0.97	0.00	-5.30	5.30	down	yes
46	5490068	NM_153259.2	255231	ILMN_16604	MCOLN2	2.53	0.14	0.00	-5.24	5.24	down	yes
47	4570768	NM_005658.3	7185	ILMN_16982	TRAF1	3.16	0.78	0.00	-5.19	5.19	down	yes
48	450189	NM_199139.1	54739	ILMN_17426	XAF1	2.50	0.13	0.00	-5.17	5.17	down	yes
49	7000398	NM_001002010.1	51251	ILMN_17697	NT5C3	2.47	0.11	0.00	-5.13	5.13	down	yes
50	7550242	NM_003865.1	8820	ILMN_17429	HESX1	2.28	-0.06	0.00	-5.05	5.05	down	yes
51	5390239	NM_005191.3	941	ILMN_17167	CD80	2.57	0.27	0.00	-4.94	4.94	down	yes
52	1010360	NM_001024070.1	2643	ILMN_23358	GCH1	2.56	0.26	0.00	-4.91	4.91	down	yes

53	4670114	XM_001133269.1	730249	ILMN_18383	LOC730249	3.81	1.52	0.00	-4.90	4.90 down	yes
54	1740360	NM_017414.3	11274	ILMN_32404	USP18	2.39	0.11	0.00	-4.86	4.86 down	yes
55	7160373	NM_002033.2	2526	ILMN_17920	FUT4	1.89	-0.38	0.00	-4.81	4.81 down	yes
56	6590445	NM_018993.2	54453	ILMN_17695	RIN2	1.85	-0.40	0.00	-4.78	4.78 down	yes
57	2510220	NM_005533.2	3430	ILMN_17453	IFI35	2.38	0.13	0.00	-4.75	4.75 down	yes
58	990768	NM_006187.2	4940	ILMN_17453	OAS3	2.43	0.19	0.00	-4.73	4.73 down	yes
59	4290189	NM_012385.1	26471	ILMN_18105	P8	2.06	-0.18	0.00	-4.73	4.73 down	yes
60	4540382	NM_020119.3	56829	ILMN_17248	ZC3HAV1	2.73	0.49	0.00	-4.72	4.72 down	yes
61	5720482	NM_016323.2	51191	ILMN_17297	HERC5	3.25	1.04	0.00	-4.64	4.64 down	yes
62	7200168	NM_006207.1	5157	ILMN_16803	PDGFRL	2.26	0.05	0.00	-4.62	4.62 down	yes
63	6650242	NM_021034.2	10410	ILMN_18057	IFITM3	2.22	0.04	0.00	-4.52	4.52 down	yes
64	2360392	NM_031212.3	81894	ILMN_17904	SLC25A28	2.02	-0.14	0.00	-4.49	4.49 down	yes
65	1260270	NM_004833.1	9447	ILMN_16813	AIM2	2.30	0.15	0.00	-4.42	4.42 down	yes
66	1410181	NM_022136.3	64092	ILMN_16848	SAMSN1	2.05	-0.09	0.00	-4.41	4.41 down	yes
67	380201	NM_012108.2	26228	ILMN_32479	STAP1	2.15	0.02	0.00	-4.37	4.37 down	yes
68	4830471	NM_024873.3	79931	ILMN_17075	TNIP3	2.39	0.29	0.00	-4.31	4.31 down	yes
69	1090390	NM_001032409.1	4938	ILMN_24108	OAS1	2.19	0.10	0.00	-4.26	4.26 down	yes
70	5960343	NM_033405.2	85441	ILMN_17875	PRIC285	2.78	0.70	0.00	-4.22	4.22 down	yes
71	870408	NM_000585.2	3600	ILMN_17241	IL15	2.30	0.24	0.00	-4.19	4.19 down	yes
72	3180681	NR_003187.1	654817	ILMN_21129	NCF1C	1.60	-0.46	0.00	-4.19	4.19 down	yes
73	3170091	NM_153236.3	168537	ILMN_17766	GIMAP7	1.46	-0.60	0.00	-4.17	4.17 down	yes
74	3940438	NM_000265.4	653361	ILMN_16973	NCF1	1.39	-0.67	0.00	-4.17	4.17 down	yes
75	5260070	NM_021170.2	57801	ILMN_16534	HES4	2.61	0.55	0.00	-4.17	4.17 down	yes
76	3840593	NM_004510.2	3431	ILMN_24151	SP110	2.20	0.15	0.00	-4.16	4.16 down	yes
77	1340491	NM_004510.2	3431	ILMN_17314	SP110	2.19	0.14	0.00	-4.15	4.15 down	yes
78	3370138	NM_152854.2	958	ILMN_23678	CD40	2.25	0.20	0.00	-4.14	4.14 down	yes
79	3990170	NM_005532.3	3429	ILMN_20587	IFI27	1.96	-0.07	0.00	-4.07	4.07 down	yes
80	540671	NM_001080978.1	10288	ILMN_23123	LILRB2	1.14	-0.88	0.00	-4.05	4.05 down	yes
81	7040035	NM_001032409.1	4938	ILMN_16756	OAS1	2.14	0.14	0.00	-4.02	4.02 down	yes
82	4040576	NM_000600.1	3569	ILMN_16996	IL6	3.34	1.35	0.00	-3.96	3.96 down	yes
83	2480577	NM_002600.3	5142	ILMN_23402	PDE4B	2.05	0.07	0.00	-3.95	3.95 down	yes
84	620403	NR_003133.1	400759	ILMN_17824	LOC400759	2.06	0.10	0.00	-3.90	3.90 down	yes
85	1230767	NM_006435.2	10581	ILMN_16733	IFITM2	2.04	0.10	0.00	-3.86	3.86 down	yes
86	2690435	NM_001548.2	3434	ILMN_16993	IFIT1	2.04	0.12	0.00	-3.80	3.80 down	yes
87	3890609	NM_021105.1	5359	ILMN_17452	PLSCR1	1.98	0.06	0.00	-3.79	3.79 down	yes
88	5810136	NM_003037.1	6504	ILMN_17707	SLAMF1	2.30	0.38	0.00	-3.77	3.77 down	yes
89	630091	NM_181782.2	135112	ILMN_16877	NCOA7	1.70	-0.21	0.00	-3.77	3.77 down	yes
90	5870692	NM_013345.2	29933	ILMN_18111	GPR132	2.06	0.15	0.00	-3.75	3.75 down	yes
91	4730059	NM_138456.3	116071	ILMN_16902	BATF2	1.97	0.08	0.00	-3.73	3.73 down	yes
92	1450427	NM_022147.2	64108	ILMN_21739	RTP4	2.03	0.14	0.00	-3.72	3.72 down	yes
93	3450180	NM_002534.2	4938	ILMN_16582	OAS1	2.03	0.13	0.00	-3.72	3.72 down	yes
94	5960747	NM_006074.3	10346	ILMN_17792	TRIM22	1.92	0.04	0.00	-3.67	3.67 down	yes
95	2710575	NM_001781.1	969	ILMN_21883	CD69	1.87	0.02	0.00	-3.62	3.62 down	yes
96	4490053	NM_001558.2	3587	ILMN_16528	IL10RA	1.97	0.12	0.00	-3.60	3.60 down	yes
97	3830349	NM_002185.2	3575	ILMN_23425	IL7R	2.08	0.23	0.00	-3.60	3.60 down	yes
98	2690689	NM_002214.2	3696	ILMN_17329	ITGB8	1.93	0.11	0.00	-3.55	3.55 down	yes
99	4390059	NM_176796.1	5031	ILMN_16600	P2RY6	1.11	-0.70	0.00	-3.52	3.52 down	yes
100	650328	NM_003327.2	7293	ILMN_21122	TNFRSF4	1.71	-0.10	0.00	-3.52	3.52 down	yes
101	1570484	NM_012068.3	22809	ILMN_16691	ATF5	1.75	-0.07	0.00	-3.52	3.52 down	yes
102	770538	NM_153374.1	256586	ILMN_17244	LYSMD2	1.32	-0.48	0.00	-3.49	3.49 down	yes
103	2100196	NM_005101.1	9636	ILMN_20540	ISG15	3.28	1.48	0.00	-3.48	3.48 down	yes
104	1440564	NM_004350.2	864	ILMN_17874	RUNX3	1.13	-0.67	0.00	-3.47	3.47 down	yes
105	2360348	NM_207315.2	129607	ILMN_17836	CMPK2	1.85	0.06	0.00	-3.47	3.47 down	yes
106	1190026	NM_021822.1	60489	ILMN_18021	APOBEC3G	1.69	-0.10	0.00	-3.45	3.45 down	yes
107	4290368	NM_024430.2	9050	ILMN_17130	PSTPIP2	1.47	-0.30	0.00	-3.42	3.42 down	yes

108	940356	NM_002189.2	3601	ILMN_16656	IL15RA	1.86	0.09	0.00	-3.42	3.42	down	yes
109	4610364	NM_006273.2	6354	ILMN_16834	CCL7	1.69	-0.08	0.00	-3.41	3.41	down	yes
110	1190040	NM_175571.2	155038	ILMN_17473	GIMAP8	1.21	-0.55	0.00	-3.40	3.40	down	yes
111	2120079	NM_002759.1	5610	ILMN_17065	EIF2AK2	1.86	0.10	0.00	-3.39	3.39	down	yes
112	6420520	NM_001250.4	958	ILMN_17792	CD40	1.97	0.21	0.00	-3.39	3.39	down	yes
113	1240142	NM_017654.2	54809	ILMN_18143	SAMD9	1.92	0.17	0.00	-3.35	3.35	down	yes
114	6200672	NM_016118.3	51667	ILMN_16652	NUB1	1.72	-0.02	0.00	-3.35	3.35	down	yes
115	2900725	NM_000785.3	1594	ILMN_17404	CYP27B1	1.78	0.04	0.00	-3.34	3.34	down	yes
116	6060468	NM_002964.3	6279	ILMN_17298	S100A8	0.30	-1.43	0.00	-3.34	3.34	down	yes
117	7560440	NM_000675.3	135	ILMN_18073	ADORA2A	2.27	0.53	0.00	-3.33	3.33	down	yes
118	2320598	NM_000266.1	4693	ILMN_17948	NDP	1.60	-0.13	0.00	-3.31	3.31	down	yes
119	3890523	XM_937367.1	3575	ILMN_16913	IL7R	2.02	0.29	0.00	-3.30	3.30	down	yes
120	3870594	NM_005531.1	3428	ILMN_17109	IFI16	1.56	-0.16	0.00	-3.30	3.30	down	yes
121	7320561	NM_016817.2	4939	ILMN_16740	OAS2	2.30	0.58	0.00	-3.30	3.30	down	yes
122	7040431	NM_020226.3	56978	ILMN_18020	PRDM8	1.81	0.09	0.00	-3.28	3.28	down	yes
123	2370639	NM_138441.2	115004	ILMN_17066	C6orf150	1.66	-0.04	0.00	-3.25	3.25	down	yes
124	4040397	NM_002608.1	5155	ILMN_17758	PDGFB	1.73	0.04	0.00	-3.23	3.23	down	yes
125	5290465	NM_033339.3	840	ILMN_23737	CASP7	1.74	0.06	0.00	-3.22	3.22	down	yes
126	3930681	NM_024119.2	79132	ILMN_16784	DHX58	2.01	0.33	0.00	-3.20	3.20	down	yes
127	5670465	NM_001124.1	133	ILMN_17089	ADM	1.77	0.10	0.00	-3.19	3.19	down	yes
128	1510193	NM_152858.1	9589	ILMN_17489	WTAP	2.09	0.42	0.00	-3.18	3.18	down	yes
129	2070646	NM_020370.1	53831	ILMN_17853	GPR84	1.95	0.28	0.00	-3.16	3.16	down	yes
130	1500280	NM_001031683.1	3437	ILMN_17017	IFIT3	3.29	1.63	0.00	-3.15	3.15	down	yes
131	5220204	NM_018381.2	55337	ILMN_17504	C19orf66	1.65	-0.01	0.00	-3.15	3.15	down	yes
132	5490240	NM_181509.1	84557	ILMN_17761	MAP1LC3A	1.71	0.06	0.00	-3.14	3.14	down	yes
133	7160010	NM_015435.3	25897	ILMN_23811	RNF19A	1.63	-0.01	0.00	-3.12	3.12	down	yes
134	7320370	NM_003151.2	6775	ILMN_17852	STAT4	2.06	0.42	0.00	-3.12	3.12	down	yes
135	4830437	NM_199344.2	375035	ILMN_33076	SFT2D2	1.65	0.02	0.00	-3.10	3.10	down	yes
136	4900086	NM_178232.2	145864	ILMN_16543	HAPLN3	1.61	-0.01	0.00	-3.08	3.08	down	yes
137	5670440	NM_001561.4	3604	ILMN_18133	TNFRSF9	1.62	0.03	0.00	-3.01	3.01	down	yes
138	6510026	NM_016584.2	51561	ILMN_17156	IL23A	2.20	0.62	0.00	-3.00	3.00	down	yes
139	520360	NM_152851.1	64231	ILMN_17210	MS4A6A	0.34	-1.24	0.00	-2.99	2.99	down	yes
140	7560471	NM_145279.4	148932	ILMN_17982	MOBKL2C	1.31	-0.26	0.00	-2.96	2.96	down	yes
141	3800398	NM_018438.4	26270	ILMN_17014	FBXO6	1.65	0.09	0.00	-2.95	2.95	down	yes
142	4120369	NM_021822.1	60489	ILMN_22324	APOBEC3G	1.48	-0.08	0.00	-2.95	2.95	down	yes
143	4150692	NM_017554.1	54625	ILMN_16917	PARP14	1.75	0.19	0.00	-2.94	2.94	down	yes
144	5870180	NM_021994.2	11179	ILMN_16816	ZNF277	1.56	0.01	0.00	-2.93	2.93	down	yes
145	7510414	NM_001552.2	3487	ILMN_16658	IGFBP4	1.43	-0.12	0.00	-2.93	2.93	down	yes
146	4280497	NM_021181.3	57823	ILMN_17109	SLAMF7	2.00	0.45	0.00	-2.92	2.92	down	yes
147	7320176	NM_001295.2	1230	ILMN_16788	CCR1	0.59	-0.96	0.00	-2.92	2.92	down	yes
148	1990397	NM_004510.2	3431	ILMN_16726	SP110	1.62	0.08	0.00	-2.92	2.92	down	yes
149	3170064	NM_005931.2	4277	ILMN_17080	MICB	1.22	-0.31	0.00	-2.89	2.89	down	yes
150	4610433	NM_139314.1	51129	ILMN_17077	ANGPTL4	1.65	0.12	0.00	-2.88	2.88	down	yes
151	520059	NM_014398.2	27074	ILMN_21708	LAMP3	1.53	0.01	0.00	-2.88	2.88	down	yes
152	5310100	NM_014290.1	23424	ILMN_17052	TDRD7	1.67	0.15	0.00	-2.87	2.87	down	yes
153	6220195	NM_006399.2	10538	ILMN_16688	BATF	1.39	-0.12	0.00	-2.86	2.86	down	yes
154	3170136	NM_152703.2	219285	ILMN_17994	SAMD9L	1.77	0.26	0.00	-2.85	2.85	down	yes
155	5700735	NM_031458.1	83666	ILMN_17312	PARP9	1.71	0.20	0.00	-2.84	2.84	down	yes
156	1940064	NM_001048183.1	65979	ILMN_17365	PHACTR4	1.42	-0.06	0.00	-2.79	2.79	down	yes
157	7330523	NM_001014279.1	389289	ILMN_20986	C5orf39	1.44	-0.04	0.00	-2.79	2.79	down	yes
158	5820035	NM_004289.5	9603	ILMN_20497	NFE2L3	1.22	-0.26	0.00	-2.78	2.78	down	yes
159	3830762	NM_181724.1	338773	ILMN_17381	TMEM119	-0.24	-1.72	0.00	-2.78	2.78	down	yes
160	240722	NM_002535.2	4939	ILMN_17367	OAS2	1.67	0.21	0.00	-2.76	2.76	down	yes
161	2510672	NM_003199.2	6925	ILMN_18141	TCF4	1.18	-0.28	0.00	-2.76	2.76	down	yes
162	1940162	NM_004120.3	2634	ILMN_17740	GBP2	1.65	0.19	0.00	-2.75	2.75	down	yes

163	6130138	NM_006468.6	10623	ILMN_17956	POLR3C	1.53	0.07	0.00	-2.75	2.75 down	yes
164	1770152	NM_152851.1	64231	ILMN_23598	MS4A6A	0.32	-1.14	0.00	-2.75	2.75 down	yes
165	2120612	XM_938742.1	130367	ILMN_18113	SGPP2	1.94	0.48	0.00	-2.75	2.75 down	yes
166	6110343	NM_145898.1	6368	ILMN_16861	CCL23	1.49	0.03	0.00	-2.74	2.74 down	yes
167	4280678	NM_005410.2	6414	ILMN_17850	SEPP1	-0.15	-1.61	0.00	-2.74	2.74 down	yes
168	5490408	NM_005195.3	1052	ILMN_17820	CEBPD	1.47	0.02	0.00	-2.73	2.73 down	yes
169	3940189	NM_004972.2	3717	ILMN_16831	JAK2	1.53	0.09	0.00	-2.72	2.72 down	yes
170	1470091	NM_172174.1	3600	ILMN_23692	IL15	1.54	0.10	0.00	-2.71	2.71 down	yes
171	5080021	NM_001165.3	330	ILMN_17761	BIRC3	1.97	0.53	0.00	-2.71	2.71 down	yes
172	4220431	NM_000127.2	2131	ILMN_21299	EXT1	1.61	0.18	0.00	-2.69	2.69 down	yes
173	1030743	NM_000595.2	4049	ILMN_17954	LTA	1.47	0.05	0.00	-2.69	2.69 down	yes
174	2230204	NM_001032731.1	4939	ILMN_22489	OAS2	1.37	-0.05	0.00	-2.68	2.68 down	yes
175	3060255	NM_182962.1	330	ILMN_24056	BIRC3	1.79	0.38	0.00	-2.67	2.67 down	yes
176	6330725	NM_005178.2	602	ILMN_17105	BCL3	0.95	-0.47	0.00	-2.67	2.67 down	yes
177	6860482	NM_017912.3	55008	ILMN_16546	HERC6	1.94	0.53	0.00	-2.66	2.66 down	yes
178	4890707	NM_002856.2	5819	ILMN_17183	PVRL2	1.42	0.02	0.00	-2.64	2.64 down	yes
179	1450370	NM_018403.4	55802	ILMN_18092	DCP1A	1.45	0.06	0.00	-2.63	2.63 down	yes
180	130519	NM_005419.2	6773	ILMN_16909	STAT2	1.50	0.10	0.00	-2.63	2.63 down	yes
181	870767	NM_001130963.1	23306	ILMN_33064	TMEM194A	1.63	0.23	0.00	-2.63	2.63 down	yes
182	5390102	NM_015278.3	23328	ILMN_21859	SASH1	1.33	-0.05	0.00	-2.60	2.60 down	yes
183	6250064	NM_002198.1	3659	ILMN_17083	IRF1	2.05	0.67	0.00	-2.60	2.60 down	yes
184	2510239	NM_030961.1	81844	ILMN_16663	TRIM56	1.32	-0.05	0.00	-2.59	2.59 down	yes
185	70121	XR_040455.1	645638	ILMN_32001	LOC645638	0.91	-0.45	0.00	-2.58	2.58 down	yes
186	4880626	NM_018326.2	55303	ILMN_17484	GIMAP4	0.87	-0.50	0.00	-2.58	2.58 down	yes
187	4900239	NM_014143.2	29126	ILMN_17019	CD274	1.46	0.10	0.00	-2.57	2.57 down	yes
188	160148	NM_013410.2	205	ILMN_23380	AK3L1	1.42	0.06	0.00	-2.56	2.56 down	yes
189	2650379	NM_013372.5	26585	ILMN_17529	GREM1	1.50	0.14	0.00	-2.56	2.56 down	yes
190	2260615	NM_004698.1	9129	ILMN_17153	PRPF3	1.18	-0.18	0.00	-2.56	2.56 down	yes
191	2030767	NM_001778.2	962	ILMN_20610	CD48	1.50	0.15	0.00	-2.56	2.56 down	yes
192	1690184	NM_183419.1	25897	ILMN_18123	RNF19A	1.38	0.02	0.00	-2.56	2.56 down	yes
193	5900253	NM_018664.1	55509	ILMN_17632	BATF3	1.38	0.03	0.00	-2.55	2.55 down	yes
194	2060047	NM_004776.2	9334	ILMN_16858	B4GALT5	1.58	0.24	0.00	-2.53	2.53 down	yes
195	4610066	NM_015257.2	23306	ILMN_32288	TMEM194A	1.68	0.34	0.00	-2.53	2.53 down	yes
196	4780044	XR_037483.1	389386	ILMN_32954	LOC389386	1.31	-0.03	0.00	-2.53	2.53 down	yes
197	7610440	NM_199139.1	54739	ILMN_23705	XAF1	1.36	0.03	0.00	-2.52	2.52 down	yes
198	5810176	NM_182664.2	83593	ILMN_23629	RASSF5	1.50	0.17	0.00	-2.52	2.52 down	yes
199	6180465	NM_017585.2	11182	ILMN_17783	SLC2A6	1.59	0.26	0.00	-2.52	2.52 down	yes
200	1820053	NM_152346.1	124935	ILMN_17871	SLC43A2	0.83	-0.49	0.00	-2.51	2.51 down	yes
201	6220673	NM_015278.3	23328	ILMN_17126	SASH1	1.23	-0.09	0.00	-2.51	2.51 down	yes
202	1990487	NM_019001.2	54464	ILMN_18090	XRN1	1.32	0.01	0.00	-2.48	2.48 down	yes
203	7560593	NM_020530.3	5008	ILMN_17805	OSM	1.04	-0.26	0.00	-2.46	2.46 down	yes
204	7330392	NM_000593.5	6890	ILMN_17510	TAP1	1.53	0.23	0.00	-2.46	2.46 down	yes
205	1570129	NM_006700.1	10906	ILMN_17582	TRAFD1	1.35	0.05	0.00	-2.45	2.45 down	yes
206	1440064	AK126405		ILMN_1913060		0.41	-0.88	0.00	-2.45	2.45 down	yes
207	4640392	NM_005937.3	4302	ILMN_17187	MLLT6	0.91	-0.38	0.00	-2.45	2.45 down	yes
208	2570300	NM_006417.3	10561	ILMN_17600	IFI44	1.98	0.69	0.00	-2.44	2.44 down	yes
209	3940133	NM_017633.2	55603	ILMN_17404	FAM46A	1.13	-0.15	0.00	-2.44	2.44 down	yes
210	1240097	NM_013448.2	11177	ILMN_16583	BAZ1A	1.43	0.15	0.00	-2.44	2.44 down	yes
211	1240440	NM_006472.2	10628	ILMN_16974	TXNIP	0.07	-1.22	0.00	-2.44	2.44 down	yes
212	4570441	NM_022168.2	64135	ILMN_17813	IFIH1	1.86	0.58	0.00	-2.44	2.44 down	yes
213	650692	NM_207332.1	157697	ILMN_21046	ERICH1	1.24	-0.04	0.00	-2.43	2.43 down	yes
214	6180056	NM_014506.1	27348	ILMN_17243	TOR1B	1.31	0.03	0.00	-2.43	2.43 down	yes
215	6510735	NM_001012967.1	91351	ILMN_32439	DDX60L	1.56	0.28	0.00	-2.43	2.43 down	yes
216	6660398	NM_002003.2	2219	ILMN_16680	FCN1	0.00	-1.28	0.00	-2.43	2.43 down	yes
217	5310053	NM_002341.1	4050	ILMN_23762	LTB	1.19	-0.09	0.00	-2.42	2.42 down	yes

218	6280725 NR_003697.1	285958 ILMN_32487 C7orf40	1.29	0.02	0.00	-2.41	2.41 down	yes
219	2680079 NM_024576.3	79627 ILMN_17158 OGFRL1	1.52	0.26	0.00	-2.41	2.41 down	yes
220	1660010 NM_033034.1	85363 ILMN_17049 TRIM5	1.28	0.01	0.00	-2.40	2.40 down	yes
221	160270 NM_022003.1	53826 ILMN_17688 FXYD6	1.17	-0.09	0.00	-2.40	2.40 down	yes
222	3130358 AK096179	ILMN_1898124	1.19	-0.07	0.00	-2.39	2.39 down	yes
223	270601 NM_033055.2	64645 ILMN_17630 HIAT1	1.24	-0.01	0.00	-2.39	2.39 down	yes
224	2650564 NM_004585.3	5920 ILMN_17016 RARRES3	1.26	0.01	0.00	-2.38	2.38 down	yes
225	510520 NM_021226.2	58504 ILMN_16763 ARHGAP22	1.15	-0.11	0.00	-2.38	2.38 down	yes
226	1230224 NM_005494.2	10049 ILMN_24024 DNAJB6	1.30	0.05	0.00	-2.38	2.38 down	yes
227	6400647 NM_139265.2	30844 ILMN_17200 EHD4	1.18	-0.06	0.00	-2.38	2.38 down	yes
228	3120474 XM_371461.4	85379 ILMN_17728 KIAA1671	1.21	-0.03	0.00	-2.36	2.36 down	yes
229	1400026 XM_001714786.1	728127 ILMN_32363 CTGLF7	1.44	0.20	0.00	-2.36	2.36 down	yes
230	6580189 XR_019393.1	387820 ILMN_16908 LOC387820	1.18	-0.06	0.00	-2.36	2.36 down	yes
231	7380243 XM_001133059.1	728772 ILMN_17519 LOC728772	1.32	0.09	0.00	-2.35	2.35 down	yes
232	4880408 NM_006378.2	10507 ILMN_16875 SEMA4D	0.97	-0.26	0.00	-2.34	2.34 down	yes
233	2680100 NM_006058.3	10318 ILMN_17036 TNIP1	1.59	0.36	0.00	-2.34	2.34 down	yes
234	7210717 NM_173558.2	221472 ILMN_21150 FGD2	1.05	-0.18	0.00	-2.34	2.34 down	yes
235	7610053 NM_017631.4	55601 ILMN_17951 DDX60	1.75	0.52	0.00	-2.34	2.34 down	yes
236	2470603 NM_016374.5	51742 ILMN_22695 ARID4B	1.07	-0.15	0.00	-2.33	2.33 down	yes
237	2470092 NM_013272.2	28232 ILMN_16547 SLCO3A1	0.91	-0.31	0.00	-2.32	2.32 down	yes
238	20521 NM_032844.1	84930 ILMN_16823 MASTL	1.12	-0.10	0.00	-2.32	2.32 down	yes
239	6110020 XM_036729.5	373856 ILMN_16903 USP41	1.19	-0.03	0.00	-2.32	2.32 down	yes
240	4120114 NM_000882.2	3592 ILMN_16713 IL12A	1.19	-0.02	0.00	-2.31	2.31 down	yes
241	1940343 NM_015368.3	24145 ILMN_16978 PANX1	1.31	0.10	0.00	-2.31	2.31 down	yes
242	4150270 NM_144590.1	118932 ILMN_21325 ANKRD22	1.19	-0.01	0.00	-2.30	2.30 down	yes
243	3190430 NM_181900.2	80765 ILMN_17843 STARD5	1.19	-0.02	0.00	-2.30	2.30 down	yes
244	1440360 NM_181791.1	353345 ILMN_20923 GPR141	1.13	-0.08	0.00	-2.30	2.30 down	yes
245	1820750 NM_007315.2	6772 ILMN_16901 STAT1	1.20	0.00	0.00	-2.30	2.30 down	yes
246	7040142 NM_001032998.1	8942 ILMN_17375 KYNU	1.40	0.20	0.00	-2.30	2.30 down	yes
247	3610343 NM_002485.4	4683 ILMN_17348 NBN	1.75	0.55	0.00	-2.29	2.29 down	yes
248	1170349 NM_005558.3	3898 ILMN_17823 LAD1	1.22	0.03	0.00	-2.29	2.29 down	yes
249	1570156 NM_016817.2	4939 ILMN_17093 OAS2	1.22	0.04	0.00	-2.28	2.28 down	yes
250	6860382 NM_007346.2	11054 ILMN_17282 OGFR	1.03	-0.16	0.00	-2.27	2.27 down	yes
251	730010 NM_017825.1	54936 ILMN_18114 ADPRHL2	0.98	-0.20	0.00	-2.27	2.27 down	yes
252	5670717 NM_207332.1	157697 ILMN_17310 ERICH1	1.20	0.02	0.00	-2.27	2.27 down	yes
253	1980672 NM_000575.3	3552 ILMN_16584 IL1A	2.43	1.25	0.00	-2.27	2.27 down	yes
254	1110494 NM_015257.1	23306 ILMN_21313 TMEM194	1.36	0.18	0.00	-2.27	2.27 down	yes
255	6400176 NM_004029.2	3665 ILMN_17981 IRF7	1.90	0.72	0.00	-2.26	2.26 down	yes
256	2570079 NM_139266.1	6772 ILMN_16913 STAT1	1.21	0.04	0.00	-2.26	2.26 down	yes
257	4210630 XM_290799.7	57636 ILMN_17645 ARHGAP23	0.92	-0.26	0.00	-2.26	2.26 down	yes
258	3140707 NM_031458.1	83666 ILMN_20535 PARP9	1.23	0.06	0.00	-2.25	2.25 down	yes
259	1710753 NM_178815.3	221079 ILMN_21200 ARL5B	1.42	0.26	0.00	-2.24	2.24 down	yes
260	2470601 NM_173842.1	3557 ILMN_16897 IL1RN	0.96	-0.21	0.00	-2.24	2.24 down	yes
261	2060121 NM_000147.3	2517 ILMN_17527 FUCA1	0.02	-1.14	0.00	-2.24	2.24 down	yes
262	6660369 NM_001491.2	2651 ILMN_16803 GCNT2	1.00	-0.16	0.01	-2.23	2.23 down	yes
263	3290292 NM_015907.2	51056 ILMN_16837 LAP3	1.06	-0.10	0.00	-2.23	2.23 down	yes
264	6020255 NM_000399.2	1959 ILMN_17431 EGR2	0.24	-0.92	0.00	-2.23	2.23 down	yes
265	2850576 NM_022367.2	64218 ILMN_17027 SEMA4A	0.14	-1.02	0.00	-2.22	2.22 down	yes
266	2470093 NM_201629.1	9414 ILMN_16649 TJP2	1.05	-0.10	0.00	-2.22	2.22 down	yes
267	2320220 NM_032029.1	83953 ILMN_18017 FCAMR	1.22	0.07	0.00	-2.21	2.21 down	yes
268	7160593 NM_152542.2	152926 ILMN_20700 PPM1K	1.27	0.12	0.00	-2.21	2.21 down	yes
269	6560075 NM_003141.3	6737 ILMN_16780 TRIM21	1.27	0.13	0.00	-2.21	2.21 down	yes
270	2140746 NM_001042724.1	5819 ILMN_23373 PVRL2	1.15	0.01	0.00	-2.20	2.20 down	yes
271	1410279 NM_001006666.1	200316 ILMN_22969 APOBEC3F	1.10	-0.03	0.00	-2.19	2.19 down	yes
272	4890451 NM_023927.1	65983 ILMN_20656 GRAMD3	1.40	0.26	0.00	-2.19	2.19 down	yes

273	1190750	NM_032148.2	84102	ILMN_17471	SLC41A2	1.24	0.11	0.00	-2.18	2.18	down	yes
274	2690324	NM_033397.2	85450	ILMN_18051	ITPRIP	0.81	-0.31	0.00	-2.17	2.17	down	yes
275	4290192	NM_203464.1	205	ILMN_17640	AK3L1	1.09	-0.03	0.00	-2.17	2.17	down	yes
276	620112	NM_001079691.1	90634	ILMN_17994	N4BP2L1	1.47	0.36	0.00	-2.16	2.16	down	yes
277	7560037	NM_133471.1	170954	ILMN_17329	KIAA1949	0.88	-0.23	0.00	-2.16	2.16	down	yes
278	1030431	NM_001995.2	2180	ILMN_16845	ACSL1	1.42	0.30	0.00	-2.16	2.16	down	yes
279	6550288	NM_020231.3	56983	ILMN_18111	KTELC1	0.99	-0.12	0.00	-2.16	2.16	down	yes
280	5310358	NM_022173.1	7072	ILMN_23884	TIA1	0.94	-0.17	0.00	-2.16	2.16	down	yes
281	5810632	NM_014306.3	51493	ILMN_17959	C22orf28	1.08	-0.02	0.00	-2.16	2.16	down	yes
282	4860458	NM_023079.3	65264	ILMN_16921	UBE2Z	0.91	-0.20	0.00	-2.15	2.15	down	yes
283	2510356	NM_001974.3	2015	ILMN_17806	EMR1	1.01	-0.09	0.00	-2.15	2.15	down	yes
284	7040386	NM_001955.2	1906	ILMN_16827	EDN1	1.55	0.44	0.00	-2.15	2.15	down	yes
285	1410168	NM_001421.2	2000	ILMN_16520	ELF4	1.09	-0.01	0.00	-2.15	2.15	down	yes
286	6560373	NM_001031677.2	53917	ILMN_16778	RAB24	0.58	-0.52	0.00	-2.15	2.15	down	yes
287	4890598	NM_032430.1	84446	ILMN_21858	BRSK1	0.76	-0.34	0.00	-2.14	2.14	down	yes
288	770047	NM_018323.2	55300	ILMN_18151	PI4K2B	1.26	0.16	0.00	-2.14	2.14	down	yes
289	4200240	NM_001080391.1	6672	ILMN_22849	SP100	1.16	0.06	0.00	-2.14	2.14	down	yes
290	2070059	NM_032789.1	84875	ILMN_22620	PARP10	1.17	0.07	0.00	-2.14	2.14	down	yes
291	1690465	XR_018848.1	650369	ILMN_16836	LOC650369	1.01	-0.09	0.00	-2.14	2.14	down	yes
292	610537	NM_058184.1	54072	ILMN_16684	C21orf42	1.11	0.02	0.00	-2.13	2.13	down	yes
293	4570024	NM_004302.3	91	ILMN_22433	ACVR1B	0.79	-0.30	0.00	-2.13	2.13	down	yes
294	4560576	NM_002468.3	4615	ILMN_17385	MYD88	1.18	0.09	0.00	-2.13	2.13	down	yes
295	4570050	NM_172174.1	3600	ILMN_22730	IL15	1.09	0.01	0.00	-2.11	2.11	down	yes
296	6550133	NM_001079691.1	90634	ILMN_23446	N4BP2L1	1.48	0.40	0.00	-2.11	2.11	down	yes
297	5720039	NM_001511.1	2919	ILMN_17878	CXCL1	2.61	1.53	0.02	-2.11	2.11	down	yes
298	5360079	NM_018384.3	55340	ILMN_17693	GIMAP5	0.61	-0.46	0.00	-2.11	2.11	down	yes
299	6180253	NM_006779.2	10435	ILMN_16527	CDC42EP2	1.11	0.03	0.00	-2.11	2.11	down	yes
300	2940403	NM_001135811.1	58516	ILMN_32726	FAM60A	1.03	-0.04	0.00	-2.11	2.11	down	yes
301	1050356	NM_057159.2	1902	ILMN_17014	LPAR1	0.78	-0.29	0.00	-2.10	2.10	down	yes
302	1470382	NM_004029.2	3665	ILMN_23490	IRF7	1.56	0.50	0.00	-2.10	2.10	down	yes
303	3830709	NR_002726.1	10151	ILMN_21745	HNRNPA3P1	1.22	0.15	0.00	-2.09	2.09	down	yes
304	3870458	NM_012108.1	26228	ILMN_17810	BRDG1	1.05	-0.01	0.00	-2.09	2.09	down	yes
305	2190452	XM_938171.2	415116	ILMN_17077	PIM3	1.52	0.46	0.00	-2.08	2.08	down	yes
306	1740050	XM_495863.3	387751	ILMN_16685	GVIN1	0.84	-0.22	0.00	-2.08	2.08	down	yes
307	7400465	NM_032172.1	84132	ILMN_21156	USP42	0.98	-0.07	0.00	-2.08	2.08	down	yes
308	4280482	NM_018370.2	55332	ILMN_16693	DRAM1	1.29	0.23	0.00	-2.08	2.08	down	yes
309	2060300	NM_198467.1	222194	ILMN_17120	RSBN1L	0.96	-0.09	0.00	-2.08	2.08	down	yes
310	1740382	NM_000161.2	2643	ILMN_17888	GCH1	1.15	0.10	0.00	-2.07	2.07	down	yes
311	6840347	NM_024576.3	79627	ILMN_20957	OGFRL1	1.40	0.35	0.00	-2.07	2.07	down	yes
312	1440341	NM_172369.2	714	ILMN_17859	C1QC	-0.21	-1.25	0.00	-2.07	2.07	down	yes
313	5390615	NM_033016.1	5155	ILMN_23943	PDGFB	1.07	0.02	0.00	-2.07	2.07	down	yes
314	1260497	NM_015150.1	23180	ILMN_18007	RFTN1	1.08	0.04	0.00	-2.06	2.06	down	yes
315	4060017	NM_001080973.1	54756	ILMN_24078	IL17RD	1.26	0.22	0.00	-2.06	2.06	down	yes
316	2000022	NM_006084.4	10379	ILMN_17454	IRF9	1.09	0.05	0.00	-2.06	2.06	down	yes
317	4810187	NM_007315.2	6772	ILMN_17773	STAT1	0.93	-0.11	0.00	-2.05	2.05	down	yes
318	2320358	NM_022154.5	64116	ILMN_22335	SLC39A8	1.06	0.02	0.00	-2.05	2.05	down	yes
319	2070392	NM_018042.2	55106	ILMN_17282	SLFN12	0.80	-0.23	0.00	-2.05	2.05	down	yes
320	6400681	NM_001005176.1	11262	ILMN_22468	SP140	1.02	-0.01	0.00	-2.05	2.05	down	yes
321	3140438	NM_020895.2	57655	ILMN_17371	GRAMD1A	1.68	0.64	0.00	-2.05	2.05	down	yes
322	6100521	NM_001040443.1	51131	ILMN_17767	PHF11	1.06	0.03	0.00	-2.05	2.05	down	yes
323	6200019	NM_002258.2	3820	ILMN_20796	KLRB1	0.86	-0.17	0.00	-2.04	2.04	down	yes
324	4560541	NM_152649.1	197259	ILMN_16678	MLKL	0.91	-0.12	0.00	-2.04	2.04	down	yes
325	1740075	NM_153698.1	195827	ILMN_17172	C9orf21	0.89	-0.14	0.00	-2.04	2.04	down	yes
326	1010487	NM_006763.2	7832	ILMN_17700	BTG2	0.86	-0.17	0.00	-2.04	2.04	down	yes
327	130181	NM_144590.2	118932	ILMN_17998	ANKRD22	1.01	-0.01	0.00	-2.03	2.03	down	yes

328	5390725	NM_001050.2	6752	ILMN_21522	SSTR2	1.13	0.11	0.00	-2.03	2.03 down	yes
329	2970347	NM_033397.2	85450	ILMN_32391	ITPRIP	0.76	-0.26	0.00	-2.03	2.03 down	yes
330	4480497	NM_033130.2	89790	ILMN_16555	SIGLEC10	0.09	-0.93	0.00	-2.02	2.02 down	yes
331	5910064	NM_033093.1	85363	ILMN_24046	TRIM5	1.03	0.02	0.00	-2.02	2.02 down	yes
332	4880215	NM_001514.3	2959	ILMN_17378	GTF2B	1.19	0.18	0.00	-2.02	2.02 down	yes
333	6480360	NM_138636.2	51311	ILMN_16578	TLR8	0.71	-0.31	0.00	-2.02	2.02 down	yes
334	6370441	NM_033338.4	840	ILMN_23629	CASP7	0.99	-0.02	0.00	-2.02	2.02 down	yes
335	5900471	NM_000956.2	5732	ILMN_17039	PTGER2	0.98	-0.03	0.00	-2.01	2.01 down	yes
336	2030309	NM_001032295.1	710	ILMN_16703	SERPING1	0.92	-0.09	0.00	-2.01	2.01 down	yes
337	2450152	NM_001042453.1	51765	ILMN_23287	MST4	1.13	0.13	0.00	-2.01	2.01 down	yes
338	7200435	NM_005170.2	430	ILMN_17234	ASCL2	0.89	-0.12	0.00	-2.00	2.00 down	yes
339	150180	NM_002425.1	4319	ILMN_17418	MMP10	0.07	3.49	0.00	10.72	10.72 up	yes
340	60079	NM_006145.1	3337	ILMN_17753	DNAJB1	-1.83	1.35	0.00	9.04	9.04 up	yes
341	2710064	XM_941665.2	387763	ILMN_16774	LOC387763	0.76	3.60	0.00	7.17	7.17 up	yes
342	4670390	NM_002089.3	2920	ILMN_16826	CXCL2	1.30	3.79	0.00	5.62	5.62 up	yes
343	6770630	NM_014475.3	27294	ILMN_16892	DHDH	-0.26	2.20	0.00	5.50	5.50 up	yes
344	6620528	NM_005952.2	4501	ILMN_17751	MT1X	-1.94	0.35	0.00	4.89	4.89 up	yes
345	3060750	NM_005047.2	5711	ILMN_17209	PSMD5	0.05	2.31	0.00	4.79	4.79 up	yes
346	6860465	NM_004997.2	4608	ILMN_17052	MYBPH	-0.36	1.74	0.00	4.29	4.29 up	yes
347	3850433	NM_005346.3	3304	ILMN_16604	HSPA1B	-1.04	1.03	0.00	4.21	4.21 up	yes
348	4010086	NM_013370.2	29948	ILMN_17959	OKL38	-1.63	0.42	0.00	4.12	4.12 up	yes
349	1340075	NM_004281.3	9531	ILMN_16597	BAG3	-0.85	1.11	0.00	3.88	3.88 up	yes
350	1440408	NM_181702.1	2669	ILMN_16770	GEM	-0.18	1.68	0.00	3.65	3.65 up	yes
351	1170246	NM_181702.1	2669	ILMN_23678	GEM	-0.26	1.60	0.00	3.64	3.64 up	yes
352	3400019	NM_002923.1	5997	ILMN_21973	RGS2	-1.75	0.11	0.00	3.61	3.61 up	yes
353	430050	NM_012342.2	25805	ILMN_16914	BAMBI	0.19	2.02	0.00	3.56	3.56 up	yes
354	160092	NM_002155.3	3310	ILMN_18061	HSPA6	-1.01	0.80	0.00	3.50	3.50 up	yes
355	4220605	NM_005239.4	2114	ILMN_17201	ETS2	-0.02	1.76	0.00	3.43	3.43 up	yes
356	1430280	NM_004364.2	1050	ILMN_17157	CEBPA	-1.99	-0.23	0.00	3.40	3.40 up	yes
357	2640719	NR_001445.1	125050	ILMN_20748	RN7SK	0.01	1.77	0.00	3.38	3.38 up	yes
358	5420564	NM_005384.2	4783	ILMN_17073	NFIL3	-0.58	1.10	0.00	3.21	3.21 up	yes
359	160598	NM_006644.2	10808	ILMN_17128	HSPH1	-1.22	0.45	0.00	3.18	3.18 up	yes
360	2680110	NM_014220.2	4071	ILMN_17703	TM4SF1	0.68	2.32	0.00	3.12	3.12 up	yes
361	7100639	NM_018948.2	54206	ILMN_16655	ERRFI1	-0.61	1.02	0.00	3.11	3.11 up	yes
362	6760021	NR_003672.2	84973	ILMN_32270	SNHG7	-1.37	0.26	0.00	3.10	3.10 up	yes
363	6420040	NM_144607.3	124637	ILMN_16709	CYB5D1	-0.13	1.49	0.00	3.08	3.08 up	yes
364	5670367	NM_007350.3	22822	ILMN_32515	PHLDA1	-0.31	1.26	0.00	2.98	2.98 up	yes
365	6110736	NM_003749.2	8660	ILMN_20834	IRS2	-1.23	0.30	0.00	2.88	2.88 up	yes
366	4810520	NM_025195.2	10221	ILMN_18038	TRIB1	-0.97	0.55	0.00	2.86	2.86 up	yes
367	4070017	NM_002539.1	4953	ILMN_17485	ODC1	-1.20	0.28	0.00	2.78	2.78 up	yes
368	990176	NR_001445.1	125050	ILMN_17394	RN7SK	0.05	1.50	0.00	2.72	2.72 up	yes
369	780711	NM_194293.2	165904	ILMN_18021	XIRP1	0.25	1.66	0.00	2.65	2.65 up	yes
370	6270273	NM_006558.1	10656	ILMN_16917	KHDRBS3	-0.14	1.20	0.00	2.54	2.54 up	yes
371	430674	NM_015193.3	23237	ILMN_17111	ARC	-0.22	1.11	0.00	2.52	2.52 up	yes
372	7550066	NM_006343.2	10461	ILMN_21385	MERTK	-1.47	-0.15	0.00	2.49	2.49 up	yes
373	3180008	NM_207501.1	401281	ILMN_17974	FLJ27255	-0.18	1.14	0.00	2.49	2.49 up	yes
374	2970482	NR_004400.1	26863	ILMN_32366	RNU1-5	0.12	1.43	0.00	2.48	2.48 up	yes
375	380685	NR_006882.1	780854	ILMN_32423	SNORD3D	0.00	1.30	0.00	2.46	2.46 up	yes
376	940152	NM_017572.2	2872	ILMN_23470	MKNK2	-0.77	0.51	0.00	2.43	2.43 up	yes
377	2510164	NR_006880.1	780851	ILMN_32395	SNORD3A	0.01	1.28	0.00	2.42	2.42 up	yes
378	1240386	NM_014851.2	9903	ILMN_16927	KLHL21	-0.85	0.40	0.00	2.36	2.36 up	yes
379	6480091	NM_018602.2	55466	ILMN_17769	DNAJA4	-0.61	0.63	0.00	2.36	2.36 up	yes
380	3780717	NM_080725.1	140809	ILMN_18048	SRXN1	-0.86	0.36	0.00	2.34	2.34 up	yes
381	4570458	NM_001010990.1	9709	ILMN_23741	HERPUD1	-0.60	0.62	0.00	2.33	2.33 up	yes
382	2360091	NR_004426.1	26864	ILMN_32446	RNU1G2	0.00	1.22	0.00	2.33	2.33 up	yes

383	1440296 NM_005324.3	3021 ILMN_16957 H3F3B	-0.82	0.40	0.00	2.32	2.32 up	yes
384	160504 XR_041703.1	728537 ILMN_32985 LOC728537	-0.04	1.17	0.00	2.30	2.30 up	yes
385	430546 NM_003518.3	8339 ILMN_17161 HIST1H2BG	-0.23	0.97	0.00	2.29	2.29 up	yes
386	6200692 NM_201559.2	2309 ILMN_16817 FOXO3	-0.23	0.95	0.00	2.27	2.27 up	yes
387	4610189 NM_001010990.1	9709 ILMN_23741 HERPUD1	-0.66	0.53	0.00	2.27	2.27 up	yes
388	6380717 NM_005345.4	3303 ILMN_17890 HSPA1A	-0.60	0.58	0.00	2.26	2.26 up	yes
389	1690630 NM_153690.4	131583 ILMN_17060 FAM43A	-0.41	0.76	0.00	2.25	2.25 up	yes
390	3990497 NR_002987.1	677838 ILMN_32454 SNORA61	-1.34	-0.17	0.00	2.24	2.24 up	yes
391	5670152 NR_004408.1	26869 ILMN_32462 RNU1-3	0.05	1.20	0.00	2.22	2.22 up	yes
392	5270110 NM_014740.2	9775 ILMN_16670 EIF4A3	-0.63	0.52	0.00	2.22	2.22 up	yes
393	3890521 NM_133328.2	162989 ILMN_17680 DEDD2	-0.99	0.13	0.00	2.17	2.17 up	yes
394	2710402 NM_015144.2	23174 ILMN_17434 ZCCHC14	-0.84	0.28	0.00	2.17	2.17 up	yes
395	6620753 NM_006007.1	7763 ILMN_17952 ZFAND5	-1.02	0.10	0.00	2.17	2.17 up	yes
396	6370523 NM_032505.1	84541 ILMN_17162 KBTBD8	-0.35	0.77	0.00	2.17	2.17 up	yes
397	5720278 NR_003098.1	23642 ILMN_32367 SNHG1	-1.13	-0.01	0.00	2.17	2.17 up	yes
398	3440138 NM_004071.2	1195 ILMN_16797 CLK1	-0.69	0.42	0.00	2.16	2.16 up	yes
399	4850136 XR_018287.2	399988 ILMN_32003 LOC399988	-0.59	0.52	0.00	2.16	2.16 up	yes
400	4290072 NM_013376.3	29950 ILMN_17940 SERTAD1	-0.52	0.58	0.00	2.15	2.15 up	yes
401	4610021 NM_003259.2	7087 ILMN_18025 ICAM5	-0.09	1.00	0.00	2.14	2.14 up	yes
402	3180450 NM_014117.2	29035 ILMN_17734 C16orf72	-0.83	0.25	0.00	2.12	2.12 up	yes
403	2570220 NR_023371.1	100169760 ILMN_32347 RN5S9	0.22	1.30	0.00	2.12	2.12 up	yes
404	620202 NM_182980.2	29948 ILMN_23195 OSGIN1	-0.75	0.32	0.00	2.11	2.11 up	yes
405	3830653 NM_006736.5	3300 ILMN_23909 DNAJB2	-0.97	0.09	0.00	2.08	2.08 up	yes
406	830619 NM_004083.4	1649 ILMN_16769 DDIT3	-0.49	0.57	0.00	2.08	2.08 up	yes
407	3360224 NM_002421.2	4312 ILMN_17264 MMP1	0.02	1.05	0.00	2.05	2.05 up	yes
408	6620201 NM_017644.3	54800 ILMN_16786 KLHL24	-1.05	-0.02	0.01	2.04	2.04 up	yes
409	3800463 NM_018344.3	55315 ILMN_17173 SLC29A3	-1.09	-0.06	0.00	2.04	2.04 up	yes
410	4920110 NM_015675.2	4616 ILMN_17189 GADD45B	0.50	1.53	0.00	2.04	2.04 up	yes
411	2650390 NM_002309.2	3976 ILMN_17387 LIF	0.18	1.20	0.00	2.03	2.03 up	yes
412	5720059 NM_018988.2	54438 ILMN_17782 GFOD1	-1.01	0.00	0.00	2.02	2.02 up	yes
413	2970128 NM_025218.2	80329 ILMN_17384 ULBP1	-0.17	0.84	0.00	2.02	2.02 up	yes
414	2650019 NM_016605.1	51307 ILMN_17445 FAM53C	-0.40	0.62	0.00	2.02	2.02 up	yes
415	780528 NM_001827.1	1164 ILMN_20722 CKS2	-0.67	0.34	0.00	2.01	2.01 up	yes
416	4200379 NR_004407.1	26824 ILMN_32451 RNU11	-0.14	0.87	0.00	2.01	2.01 up	yes